Laser spectroscopic investigation of sulfur-centered intermolecular interactions in the gas phase

博士論文

Laser Spectroscopic Investigation of Sulfur-Centered Intermolecular Interactions in the Gas Phase

（硫黄を含む分子間相互作用の気相レーザー分光研究）

王丹丹

平成 30 年

Acknowledgements

I would like to express my gratitude to all those helped me during this three years study in Japan. The study in Japan is my greatest treasure in life.

First, I wish to express my most sincere appreciate to Professor **Asuka Fujii**, who was my supervisor. His enthusiastic advice, encouragement and support have definitely made a mark in my life. During these three years, not only he taught me the professional knowledge, experimental skills and the way of thinking, but also impressed me very much on the attitude towards scientific work, which will benefit me all through my life. Besides, he showed great patience and responsibilities to my work which let me go over many difficulties in the research including experiment, presentation, proposal, writing paper and so on.

I greatly thank **Professor Yoshiyuki Matsuda** and **Professor Toshihiko Maeyama** for helpful discussion in the seminar. Their in-depth and comprehensive discussions give me many constructive suggestions. It's their help that made many tough problems encountered clear and gave me confidence to go forward.

Deep thanks also go to all the other group members in the Quantum Chemistry Laboratory and the people I met in Japan, for their kindness and helps in my life.

At last I want to thank my beloved family parents for their moral support on me all through these years, especially, indebted to my husband **Weiguang Peng** for his love, trust, support and encouragement.

Dandan Wang

Contents

Acknowledgements II

Chapter 1 General introduction 1

1.1 Noncovalent interactions 2

1.2 Hemibond 5

Reference 11

Chapter 2

Structures of protonated hydrogen sulfide clusters, $H^+(H_2S)_n$, highlighting the nature of sulfur-centered intermolecular interactions 16

2.1 Introduction 17

2.2 Experiment Setup 18

2.4 Results and disscussion 26

Reference 53

Chapter 3

Spectroscopic observation of hemibonded (two-center three-electron bonded) structures of $(H_2S)_n^+$ clusters in the gas phase 57

3.1 Introduction 58

3.2 Experimental Setup 60

3.3 Results and Discussion 61

3.4 conclusions 75

Reference 75

Summary 77

Chapter 1

General introduction

Abstract

Sulfur is a biologically abundant element, like amino acids, disulfide bridges, etc. The existence of the sulfur-centered hydrogen bond (SCHB) has been well established by crystallographic data of protein and organic molecules. The role of SCHB in stabilization of protein structures and selective binding of ligands at the active site of proteins is profound, while the understanding of such particular weak interaction is rather scarce, especially from the aspect of molecular level in the gas phase. Even though it has been figured out that sulfur is incompetent in forming a strong and typical HB due to its weak electronegativity, surprisingly, it is capable of engaging in other significant and versatile intermolecular bonds, for instance, chalcogen bond (or more generally, σ hole interaction), lone pair-π interaction (intrinsically, π hole interaction), hemibond in radical cations, and so on. However, so far, we could hardly look insight into their nature due to experimental difficulties in molecular-level characterization. In this thesis, we aim at resolving these problems, mainly focusing on SCHB and hemibonds, by infrared photodissociation spectroscopy in the gas phase and quantum-chemical calculations.

1.1 Noncovalent interactions

Noncovalent interactions have been the subject of inquiry for many years, because of their critical importance in a multitude of chemical and biological phenomena.[1] All the noncovalent interactions can be classified by four fundamental physical contributions: electrostatic, induction, dispersion, and exchange interaction, and the nature of the interaction varies by proportions of these ingredients. The quantitative analysis can be realized by computational methods providing a rigorous quantitative quantum mechanical description of noncovalent interactions, for example, the symmetry adapted perturbation theory (SAPT) program. As a qualitative understanding, the interaction of two nonpolar species is usually dominated by dispersion, while the interaction of charged or highly polar entities is primarily governed by electrostatic force. In both the cases, exchange repulsion is competing with the attractive interactions, and their balance determines the equilibrium intermolecular structure. Among noncovalent interactions, a hydrogen bond (HB) is the most well-explored one, which is formed between an electron-deficient hydrogen covalently bound to an electronegative atom and a region of high electron density, denoted as AH•••D (A refers to the electron acceptor and D to the donor).[2]

Regular HBs have been fairly well understood. On the other hand, sulfur centered hydrogen bonds (SCHBs) have been overlooked, and many queries remain with respect to them. The large difference in electronegativity of sulfur (2.58) and oxygen (3.44) and the small difference in that of S and H (2.20) have resulted in a general awareness for a long time that SCHBs should not be classified to a conventional HB and SCHBs should be a

weak intermolecular interaction. However, is this truth? With the progress of investigations, such understanding has been challenged.[3] Characterization of SCHBs by model molecular clusters has revealed that SCHBs have many properties different from typical H-bonds.[3-7] By the matrix-isolation IR spectroscopy, it has been reported that the strength of the S•••H−O and O•••H−O HBs are very close to each other for DMS-HNO_3 and DME-HNO_3.[4] Wategaonkar and coworkers have emphasized that dispersion plays a major role to generate attraction in the O−H···S hydrogen bond.[4] Sulfur not only forms σ-type HBs, like S•••H−N and S•••H−S, but also can be engaged in π-type HBs, for instance, S−H•••π formed between H_2S and benzene. It has been theoretically proved that the magnitude of the S−H•••π interaction is the largest one among the X−H•••π (X = C, N, O, and S) type interactions[5,8] and dispersion has been concluded to make a significant contribution to the S−H•••π-type interaction. The investigation of SCHBs has covered many organic crystals, peptides, and protein, as well as their roles in biomolecular structures and functions.[9] The geometric characteristic and strength of SCHBs vary in different systems, and the underlying mechanism of their particularity and diversity are still obscure.

The σ-hole and π-hole interactions also have recently become popular topics in many fields. The σ-hole bond has been initially known as the halogen bond, however, its essence can be expanded extensively by substitution of a halogen element to a chalcogen or pnicogen element.[10] The halogen bond refers to a net attractive interaction between an electrophilic region associated with a halogen atom in a molecular entity and a nucleophilic region in another or the same molecular entity, and it is electrostatic in nature. Basically, such an interaction is due to the polarization of the atom's electronic charge toward the

covalent bonds that it forms. According to the definition of the σ-hole bond, if we change the positive electrostatic potential moiety to the special π system with the π-electron-deficient cavity, a π-hole interaction could occur. Such an interaction is proved by a strong complex formed between C_6F_6 and Cl^-.[11] This interaction is also called *n*-π (lone pair-π) interaction. The directionality of the σ-hole bond (Y−X•••A) refers to the angle between the Y−X covalent bond and the vector direction from the center of the σ-hole in X to the bond acceptor (A). Similarly, the directionality of the π-hole bond refers to the angle formed between the π-framework plane and the vector direction from the center of the π-hole (or interacting atom(s) to the bond acceptor−it resembles a mortise−tenon joint structure.[12] The participation of a sulfur atom occupies a large proportion of these σ-hole interactions because of the abundance of sulfur in biochemistry field. For instance, the theoretical investigation of the S•••S interaction formed between $H_3C-S-CH_3$ and H_3C-S-Z (Z=CH_3, C_2H, CN) has revealed the existence of σ-hole contact;[13] The S•••N bond in FHS•••NH_3 complex with the binding energy of around 8 kcal/mol, which is stronger than H-bond SH•••N, has been proposed by the theoretical calculation.[14] Some particular cases of sulfur-containing noncovalent interactions also have drawn great interest. As has been found in the calculation performed on $(X_2CS)_2$ dimers, a sulfur atom generate a negative σ-hole where X=−NH_2, −OH, and a positive σ-hole where X=−F, −Cl, and the C=S•••S=C contact is generally dominated by the dispersive component.[15] All these phenomenon are charming to scientist, while we still have little knowledge on them. Especially from a spectroscopic view in the gas phase, more experimental works can be planned.

1.2 Hemibond

When we go further on the sulfur-containing intermolecular interactions, a significant notion will be put forward, that is hemibond, a particular covalent bond prevalently exists in (cation) radical systems.

A radical cation with an unpaired electron in p orbital could be stabilized by coordination with a free p-electron pair of another unoxidized molecule. Such an interaction is called hemibond or two-center three-electron (2c-3e) bond. Since the concept of the hemibond was first proposed by Linus Pauling in the early 1930s, hemibonds have been encountered in various areas such as free-radical chemistry, biochemistry, organic reactions, radiation chemistry, and so on.[16-19] To elucidate the nature of hemibond, two main theories are developed. In the valence bond (VB) formalism, a hemibond is viewed as originating from the resonance between two VB structures. This means that a hemibond is more stabilized when the orbital energy difference is smaller. In other words, the closer ionization potential energies of the two counterparts will result in a stronger hermibond. Another theory is molecular orbital (MO) theory, which is extensively utilized to get insight into a hemibond. In MO theory, a hemibond is represented by two MOs formed by a linear combination of a fully occupied non-bonding orbital and a half-occupied non-bonding orbital. Typically, a lone pair p orbital of a closed shell molecule interacts with a half-occupied p orbital of a (cation) radical. One MO is bonding, and the other MO is anti-bonding. These two MOs are occupied by three electrons, and therefore, the bond order is ½. Many literatures have described the signature of hemibonds by theoretically calculated

bond length, binding energy, band order, and the degree of localization of the unpaired electron.[20] The net hemibond energy, D_e, can be expressed by,[21]

$$D_e=[3\alpha S^2+\beta-(\alpha+3\beta)S]/(1-S^2)$$

Herein, the symbols α, β, and S denote the Hűckel Coulomb, resonance, and overlap integrals respectively. Based on the Wolfsberg-Helmholtz approximation, we assume that β is proportional to S. Then, a further simplified representation is given,

$$D_e=(K-1)aS(1-3S)/(1-S^2);\ \ \beta=K\alpha S$$

It is clear that the hemibond energy is zero under the condition that overlap integral S=0 or 1/3, and the maximum D_e is achieved at S=0.17. This means that the weak overlap is favored in the hemibond bond and a longer bond is expected than a normal two-electron bond. Furthermore, D_e is approximately quadratic to S while the linear correlation is expected in a two-electron bond.

The concept of the hemibond was first proposed by L. Pauling to interpret the stability of some simple chemical systems like NO, NO_2, O_2, and He_2^+.[22] Let us start from the quintessential example, He_2^+ shown in Fig. 1.1. The 1s orbitals of each He atom overlaps with that of the counterpart to form double-occupied σ bonding and single-occupied σ*

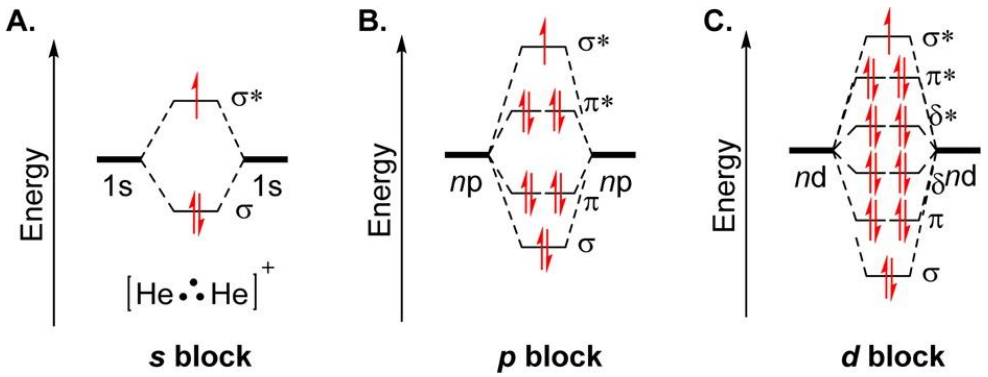

Fig. 1.1 Molecular orbital schemes for 2c/3e bonds formed by overlap of two orbitals. (A) He_2^+, the two s orbital overlap (B) the p orbitals overlap (C) the d orbital overlap. Reproduced from Ref. 28 with permission from the Acc. Chem. Res. Owner Societies.

antibonding orbitals. By the similar manner, the alkaline earth metal dimer cations[23-24] and group 12 dimer cations[25-26] also form their hemibonds by overlap of two s orbitals. Next, the concept of the hemibond was extended to radical cation dimers in the p or d block elements. For the p block species, the monocationic noble gas dimers fulfill the valence electron requirement of the hemibond, where the bonding σ and two π orbitals and antiobonding π* orbital are fully-occupied along with the half-occupied σ* orbital. For Xe_2^+, the crystallographic characterization was performed and it showed the long Xe∴Xe distance, 3.09 Å.[27] As could be conceived, the overlap between d orbitals could be formed for the dimer of transition metals, like Pd_2^+. However, no experimental evidence for the hemibond structure of Pd_2^+ has been reported so far. As has been well known, coordination chemistry is a powerful avenue to stabilize unstable species. Therefore, some experimental

and theoretical studies in coordination chemistry have been reported on the hemibond consisted of transition metal.[28]

Now, we step into the species with high complexity beyond the simplest homonuclear dimer. Besides the coordination chemistry mentioned above, hemibonds including main group atoms also have attracted great interest, and they have been widely characterized. For instance, there have been many reports on $[H_nX\therefore XH_n]^+$(X=F,O,N,Cl,S,P; n=1 − 3) and $[R_2S\therefore SR_2]^+$.[29-35] $[RS\therefore SR]^-$[36] We should notice that most of the hemibonded systems are charged ones, and the excess charge complicates the understanding of the bonding with the coexistence of the electrostatic interaction. Therefore, there have been some investigations of neutral radicals, like X•••H_2O (X=F, Cl, Br and OH),[37] H_2S•••X (X=F, Cl, Br and OH)[38] and more generally all kinds of X∴Y hemibond (X and Y = N, S, P, halogen, and etc.).[39-43]

We also could find some more complicated cases of hemibonds, like cations of 1,5-dithiocane (Fig. 1.2 (A)) and 1,8-chalcogen naphthalenes (e.g., $Nap(SPh)_2$ in Fig. 1.2(B)).[44-45] In these systems, the unpaired electron is p-localized over two equivalent sulfur atom. Actually, we could expand the two-centered three electron structure to many-nuclei systems, especially containing aromatic ring, where the unpaired electron is π-delocalized over more than two atoms.[46] If the system is centrosymmetric, it is regarded as a special case of two-centered three electron bonds described by Pauling.

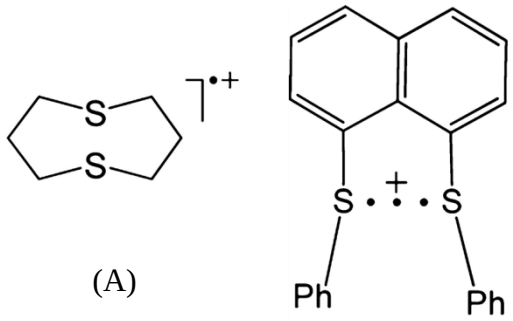

(A) (B)

Fig. 1.2 Two complicated cases of hemibonded structures.

Recently, biochemical importance of multi-centered three electron bonds has been pointed out. A critical role of hemibond has been proposed in the hopping mechanism of electron transfer in the biological process. For instance, the temporary formation of hemibonds, like O∴O, O∴S, can serve as relay stations in the long-range electron (hole) transport in protein.[47] Besides these p block hemibonds, one particular type also has attracted much interest. This is the S∴π interaction. The neighboring aromatic rings can favor the side chain of methionine (Met) or cysteine (Cys) residues (two sulfur-containing

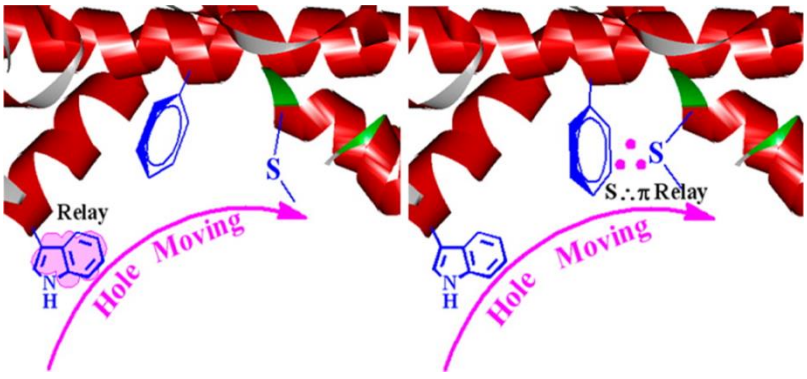

Fig. 1.3 Electron transfer through the S∴π relay station in proteins. Reproduced from Ref. 48 with permission from the J. Phys. Chem. C Owner Societies.

amino acids) to take part in the electron transfer by forming the $S\therefore\pi$ relay station in proteins (as shown in Fig. 1.3). Because of the moderate binding energies of $S\therefore\pi$, the self-movement of the protein is able to break this bonding and promotes the electron hole transfer.[48-49] However, such a multi centered three electron bond has rarely been investigated.[50-52]

Among the enormous studies of hemibonds, the most extensively studied system is sulfur-sulfur centered radical cations due to its key role in organic reactions and biological process as intermediates (such as shown in Fig. 1.2). The experimental observation of the sulfur-sulfur hemibond has been pioneered by Asmus and coworkers.[53-58] In 1975, They found the formation of transient radical cation $(R_2S_2)^+$ upon oxidation of 1,4-dithian by OH radicals in aqueous solutions at low solute concentration, through the observation of the transient absorption due to the σ*-σ electronic transition.[53] Then, through both Fourier transform ion cyclotron resonance (FTICR) and tandem mass spectrometry (MSMS), the stable dimer cation formation by ionizing di-isopropyl sulphide with its neutral analogue in the gas phase was observed. The hemibond formation in the gas phase has been proposed for the first time on the basis of the fragmentation pattern.[57] In the work of Moradi *et al*., the gas phase dimerization equilibrium measurement of dimethyl sulfide cations has also suggested formation of the S-S hemibond.[59] To verify the existence and illustrate the property of the S-S hemibond, numerous quantum chemistry calculations have been performed. As the first step towards a wider investigation of the S-S hemibond, the simplest model, $(H_2S)_2^+$ has been frequently utilized. The calculations of $(H_2S)_2^+$ have been

first performed by Clark,[60] and the series of his study has been extended to a variety of hemibonded systems.[61-63] For the detail of H_2S species, we will discuss in Chapter 3.

Reference

[1] Molecular Interactions. From Van der Waals to Strongly Bound Complexes; S. Scheiner, Ed.; Wiley: Chichester, 1997; P. Hobza, R. Zahradanik, Intermolecular Complexes; Academia: Prague, 1988.

[2] E. Arunan, G. R. Desiraju, R. A. Klein, J. Sadlej, S. Scheiner, I. Alkorta, D. C. Clary, R. H. Crabtree, J. J. Dannenberg, P. Hobza, et al. *Pure Appl. Chem.* 2011, **83**, 1637-1641.

[3] H. S. Biswal, S. Bhattacharyya, A. Bhattacherjee and S. Wategaonkar, *Int. Rev. Phys. Chem.* 2015, **34**, 99-160.

[4] H. S. Biswal, P. R. Shirhatti and S. Wategaonkar, *J. Phys. Chem. A* 2010, **114**, 6944-6955.

[5] H. S. Biswal and S. Wategaonka, *J. Phys. Chem. A* 2009, **113**, 12774-12782.

[6] Bhattacherjee, Y. Matsuda, A. Fujii and S. Wategaonkar, *J. Phys. Chem. A* 2015, ***119,*** 1117-1126.

[7] V. R. Mundlapati, S. Ghosh, A. Bhattacherjee, P. Tiwari and H. S. Biswal, *J. Phys. Chem. Lett.* 2015, **6**, 1385-1389.

[8] M. Wierzejewska, *J. Mol. Struct.* 2000, **520**, 199-214.

[9] (a) N. Ueyama, N. Nishikawa, Y. Yamada, T. Okamura, S. Oka, H. Sakurai, and A. Nakamura, *Inorg. Chem.* 1998, **37**, 2415-2421. (b) A. Nangia and G.R. Desiraju, *J. Mol.*

Struct. 1999, **474**, 65-79. (c) J. M. Word, S. C. Lovell, T. H. LaBean, H. C. Taylor, M. E. Zalis, B. K. Presley, J. S. Richardson, and D. C. Richardson, *J. Mol. Biol.* 1999, **285**, 1711-1733. (d) J. M. Word, S. C. Lovell, J. S. Richardson, and D. C. Richardson, J. Mol. Biol. 1999, **285**, 1735. (e) K. E. Ranaghan, J. E. Hung, G. J. Bartlett, T. J. Mooibroek, J. N. Harvey, D. N. Woolfson, W. A. van der Donk, and A. J. Mulholland, *Chem. Sci.* 2014, **5**, 2191-2199. (f) T. Steiner, Acta Crystallogr., Sect. C: Cryst. Struct. 2000, **56**, 876-877. (g) B. W. Beck, Q. Xie, and T. Ichiye, *Biophys. J.* 2001.**81**, 601-613.

[10] H. Wang, W. Wang and W. J. Jin, *Chem. Rev*. 2016, **116**, 5072-5104.

[11] (a) K. Hiraoka, S. Mizuse, S. Yamabe, *J. Phys. Chem.* 1987, **91**, 5294-5297. (b) S. Chowdhury, P. Kebarle, *J. Chem. Phys.* 1986, **85**, 4989-4994.

[12] K. Eskandari, H. Zariny, *Chem. Phys. Lett*. 2010, **492**, 9-13.

[13] C. Bleiholder, D. B. Werz, H. Köppel, and R. Gleiter, *J. Am. Chem. Soc.* 2006, **128**, 2666-2674.

[14] U. Adhikari and S. Scheiner, *J. Phys. Chem. A* 2012, **116**, 3487-3497.

[15] R. Shukla and D. Chopra, *Cryst. Growth. Des.* 2016, **16**, 6734-6742.

[16] (a) S. A. Chaudhri, M. Göbl, T. Freyholdt, K. D. Asmus, *J. Am. Chem. Soc.* 1984, **106**, 5988-5992. b) M. Bonifacic, J. Weiss, S. A. Chaudhri, K. D. Asmus, *J. Phys. Chem.* 1985, **89**, 3910-3914.

[17] L. K. Steffen, R. S. Glass, M. Sabahi, G. S. Wilson, C. Schöneich, S. Mahling, K. D. Asmus, *J. Am. Chem. Soc.* 1991, **113**, 2141-2145.

[18] (a) W. K. Musker, *Acc. Chem. Res.* 1980, **13**, 200-206. (b) M. Tamaoki, S. Masanori, Y. Shiratori, K. Itoh, *J. Phys. Chem.* 1989, **93**, 6052-6058 and references therein.

[19] X. Qin, Q. Meng, F. Williams, *J. Am. Chem. Soc.* 1987, **109**, 6778-6795.

[20] D. K. Maity, *J Phys. Chem. A* 2002, **106**, 5716-5721.

[21] P. M. W. Gill and L. Radom. *J. Am. Chem. Soc.* 1988, **110**, 4931-4941.

[22] L. Pauling, The nature of the chemical bond, Cornell University Press, Ithaca, New York, 1960.

[23] H. Li, H. Feng, W. Sun, Y. Zhang, Q. Fan, K. A. Peterson, Y. Xie, H. F. Schaefer, *Mol. Phys.* 2013, **111**, 2292-2298 and references therein..

[24] I. O. Antonov, B. J. Barker, V. E. Bondybey, M. C. Heaven, *J. Chem. Phys.* 2010, **133**, 074309.

[25] G. L. Gutsev, C. W. Bauschlicher, *J. Phys. Chem. A* 2003, **107**, 4755-4767.

[26] J. Kang, J. Kim, H. Ihee, Y. S. Lee, *J. Phys. Chem. A*, 2010, **114**, 5630-5639.

[27] T. Drews, K. Seppelt, *Angew. Chem., Int. Ed. Engl.* 1997, **36**, 273-274.

[28] J. F. Berry, *Acc. Chem. Res.* 2016, **49**, 27-34.

[29] B. C. Gilbert, D. K. Hodgeman, R. O. C. Norman, *J. Chem. Soc., Perkin Trans. 2* 1973, **0**, 1748-1752.

[30] M. Bonifacic, H. Mockel, D. Bahnemann, K.-D. Asmus, *J. Chem. Soc., Perkin Trans. 2* 1975, **0**, 675-685.

[31] T. Drewello, C. B. Lebrilla, H. Schwarz, L. J. de Koning, R. H. Fokkens, N. M. M. Nibbering, E. Anklam, K.-D. Asmus, *J. Chem. Soc., Chem. Commun.* 1987, **0**, 1381-1383.

[32] A. J. Illies, P. Livant, M. L. McKee, *J. Am. Chem. Soc.* 1988, **110**, 7980-7984.

[33] S. Ekern, A. Illies, M. L. McKee, M. Peschke, *J. Am. Chem. Soc.* 1993, **115**, 12510-12518.

[34] M. C. R. Symons, *J. Chem. Soc., Perkin Trans. 2* 1974, **0**, 1618-1620.

[35] S. Zhang, X. Wang, Y. Sui, X. Wang, *J. Am. Chem. Soc.* 2014, **136**, 14666-14669.

[36] D. J. Nelson, R. L. Petersen, M. C. R. Symons, *J. Chem. Soc., Perkin Trans. 2* 1977, **0**, 2005-2015.

[37] J. Li, Y. Li, and H. Guo, *J Chem Phys.* 2013, **138**, 141102,

[38] D. M. Chipman, *J. Phys. Chem. A* 115, **7**, 1161-1171.

[39] F. Gerson, J. Knobel, U. Buser, E. Vogel, M. Zehnder, *J. Am. Chem. Soc.* 1986, **108**, 3781-3783.

[40] A. R. Lyons, M. C. R. Symons, *J. Chem. Soc., Faraday Trans. 2* 1972, **68**, 1589-1594.

[41] J. E. King, A. L. Illies, *J. Phys. Chem. A* 2004, **108**, 3581-3585.

[42] P. Livant, A. Illies, *J. Am. Chem. Soc.*1991, **113**, 1510-1513.

[43] C. P. Moradi, C. Xie, M. Kaufmann, H. Guo, G. E. Douberly, *J. Chem. Phys.* 2016, **144**, 164301.

[44] C. H. Hendon , D. R. Carbery and A. Walsh, *Chem. Sci.* 2014. **5.** 1390-1395,

[45] S. Zhang, X. Wang, Y. Sui, and X. Wang, *J Am. Chem. Soc.* 2014, **136**, 14666-14669.

[46] R. Hoffmann, A. Imamura and W. Hehre, *J. Am. Chem. Soc.* 1968, **3290**, 1499-1509.

[47] X. Chen, L. Zhang, Z. Wang, J. Li, Y. Bu, *J. Phys.Chem. B* 2008, **112**, 14302-14311.

[48] X. Chen, Y. Tao, J. Li, H. Dai, W. Sun, X. Huang, Z. Wei, *J. Phys. Chem. C* 2012, **116**, 19682-19688.

[49] N. P. A. Monney, T. Bally, G. S. Bhagavathy, R. S. Glass, *Org. Lett.* 2013, **15**, 4932-4935.

[50] W. Sun, H. Ren, Y. Tao, D. Xiao, X. Qin, L. Deng, M. Shao, J. Gao, X. Chen, *J. Phys. Chem. C* 2015, **119**, 9149-9158.

[51] W. Sun, M. Shao, H. Ren, D. Xiao, X. Qin, L. Deng, X. Chen, J. Gao, *J. Phys. Chem. C* 2015, **119**,6998-7005.

[52] W. Sun, H. Dai, Y. Tao, D. Xiao, Y. Zhang, Z. Wei, X. Chen, *J. Phys. Chem. C* 2013, **117**, 18325-18333.

[53] D. Bahnemann, K.-D. Asmus, *J. Chem. Soc., Chem. Commun.* 1975, **0**, 238-239.

[54] K.-D. Asmus, *Acc. Chem. Res.* 1979, **12**, 436-442.

[55] S. A. Chaudri, K.-D. Asmus, *Angew. Chem. Int. Ed.*1981, **20**, 672-673.

[56] M. Göbl, M. Bonifačić, K.-D. Asmus, *J. Am. Chem. Soc.* 1984, **106**, 5984-5988.

[57] T. Drewello, C. B. Lebrilla, H. Schwarz, L. J. de Koning, R. H. Fokkens, N. M. M. Nibbering, E. Anklam, K.-D. Asmus, *J. Chem. Soc., Chem. Commun.* 1987, **0**, 1381-1383.

[58] K.-D. Asmus, in Sulfur-Centered Reactive Intermediates in Chemistry and Biology, NATO-ASI Series, Series A: Life Sciences, Springer, 1990, 155-172.

[59] A. J. Illies, P. Livant, M. L. McKee, *J. Am. Chem. Soc.* 1988, **110**, 7980-7984.

[60] T. Clark, *J. Comput. Chem.* 1981, **2**, 261-265.

[61] T. Clark, *J. Comput. Chem*. 1982, **3**, 112-116.

[62] T. Clark, *J. Comput. Chem.* 1983, **4**, 404-409.

[63] T. Clark, *J. Am. Chem. Soc.* 1988, **110**, 1672-1678.

Chapter 2

Structures of protonated hydrogen sulfide clusters, $H^+(H_2S)_n$, highlighting the nature of sulfur-centered intermolecular interactions

Published in *Physical Chemistry Chemical Physics*, **2017**, 19, 2036-2043.

Abstract

Unique intermolecular structures of protonated hydrogen sulfide clusters, $H^+(H_2S)_n$, are revealed by infrared spectroscopy and *ab initio* calculations. The identified intermolecular structures are significantly different from those of corresponding protonated water clusters, $H^+(H_2O)_n$, in spite of the common hydrogen bond coordination ability between hydrogen sulfide and water. Protonated hydrogen sulfide clusters have the Eigen type ion core, H_3S^+, in the size range of $n = 3 – 9$. After the first hydrogen bonded shell formation is completed at $n = 4$, further solvation prefers a new shell bound by the charge-dipole interaction rather than the second hydrogen bonded shell. Thus, much closely solvated structures, in which 7 molecules, at maximum, directly interact with the Eigen type ion core, are formed. The

beginning of the second hydrogen bonded shell is found at n = 9. Competition among intermolecular interactions in $H^+(H_2S)_n$ is discussed.

2.1 Introduction

Extensive investigations have been conducted on protonated water clusters, $H^+(H_2O)_n$, in the gas phase, which is regarded as a powerful model system to explore structures and dynamics of the aqueous proton.[1-7] In the intermolecular structure formation of $H^+(H_2O)_n$, the hydrogen bond (H-bond) plays an essential role. The H-bond coordination property of water is obviously a key factor to understand intermolecular structures of $H^+(H_2O)_n$. Sulfur belongs to the same group as oxygen, and the H-bond coordination property of H_2S is expected to be same as that of H_2O. This raises a simple question whether the intermolecular structure of $H^+(H_2O)_n$ can be held if we replace H_2O with H_2S. Recently, because of the ubiquity and significance in biological systems, and also those in materials science, sulfur-centered hydrogen bonds (SCHBs) have received increasing interest.[8,9] As has been discussed in the Chapter 1, The properties of SCHBs are different from typical H-bonds.[10-13] These properties could easily be rationalized by comparison between the electric properties of H_2O and H_2S summarized in Table 2.1.1.[14,15] The magnitude of the proton affinity of H_2S is close to that of H_2O. The small dipole moment and large polarizability of H_2S suggest a remarkable role of dispersion and relatively less importance of electrostatic interactions in SCHBs. On the other hand, cluster studies on SCHB network structures have been surprisingly scarce.[16-20] With respect to $H^+(H_2S)_n$, a very elementary level calculation at HF/4-31G has been the unique report on their H-bond structures, so far.[21]

Table 2.1.1 Dipole moments, polarizabilities, and proton affinities of H_2O and H_2S.

	H_2O	H_2S
dipole moment / D [a]	1.855	0.978
polarizability / 10^{-24}cm^3 [a]	1.45	3.95
proton affinity / kJmol^{-1} [b]	691	705

[a] Ref. 14, [b] Ref. 15

In the present work, we perform size-selective infrared (IR) spectroscopy of protonated hydrogen sulfide clusters, $H^+(H_2S)_n$, to characterize intermolecular structures constructed by sulfur-centered intermolecular interactions. Quantum chemical calculations are also employed to analyze measured IR spectra. Characteristic intermolecular structure formation of $H^+(H_2S)_n$ is demonstrated, and the particularity and generality of sulfur-centered intermolecular interactions, in comparison with typical H-bonds of water, are discussed. Through this work, we also try to shed new light on the structure property of $H^+(H_2O)_n$ from the view point of the competition among intermolecular interactions. H_2S, which has the same H-bond coordination property as H_2O, can be an interesting reference to examine factors in construction of H-bonded water network structures.

2.2 Experiment Setup

2.2.1 Overview of infrared photodissociation spectroscopy

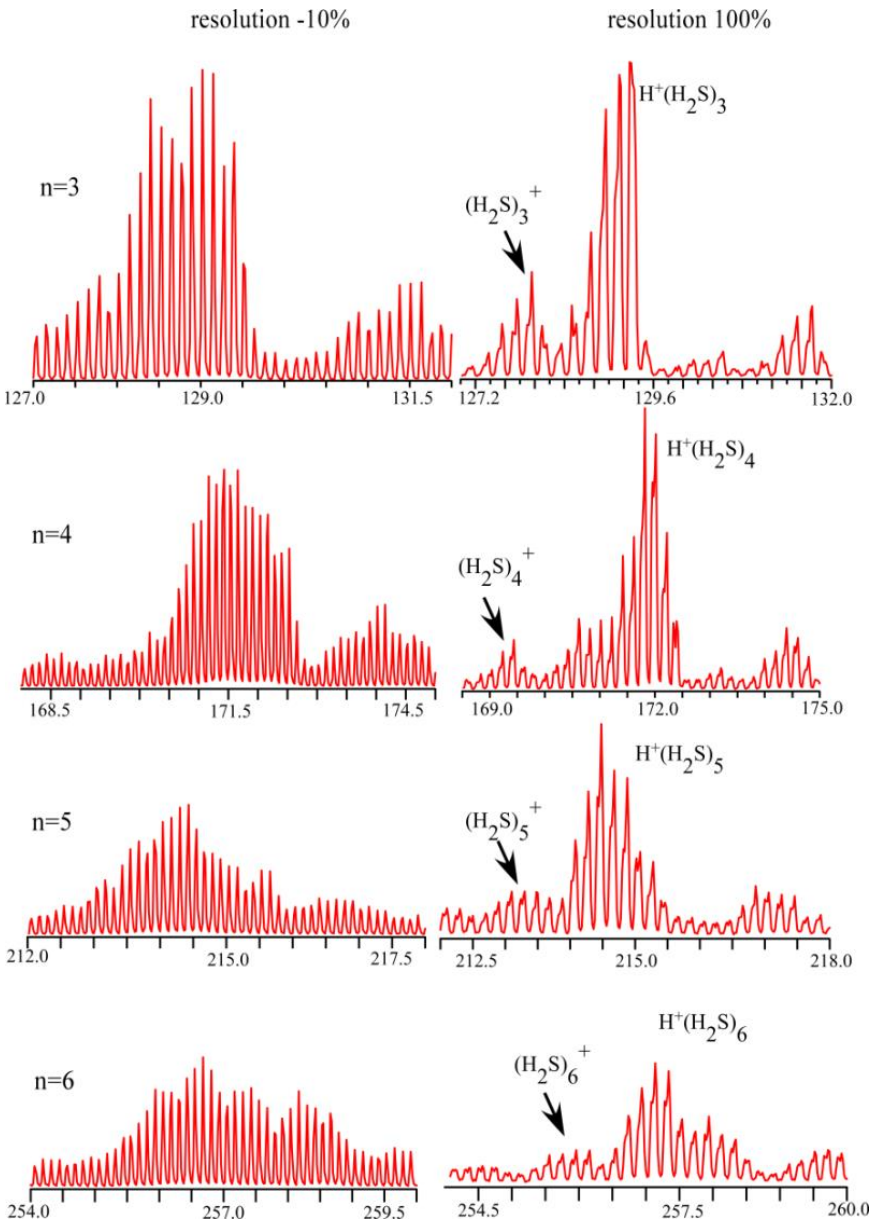

Fig. 2.2.1 The mass spectra of our cluster ion source under the resolution -10% (left panel) and 100% (right panel)

$H^+(H_2S)_n$ clusters were generated by discharge to a supersonic jet expansion of the H_2S/Ar gaseous mixture. Generated ions were introduced into the tandem type quadrupole mass spectrometer. The cluster size of interest was selected by the first mass spectrometer. The mass resolution was set to be higher than $\Delta m/z = 1$ (high mass resolution condition as shown in the right column in Fig. 2.2.1), and contribution of $(H_2S)_n^+$ radical cation clusters was carefully removed. Then, the size-selected clusters were introduced into the octopole ion guide. The clusters were irradiated by the tunable IR light from the OPO/OPA system (LaserVision) pumped by the Nd-YAG laser (Continuum PL-8000), and the fragment ions were monitored by the second quadrupole mass spectrometer. IR spectra were recorded by monitoring the fragment in the single H_2S loss channel while scanning the IR frequency in the 2300 – 2700 cm^{-1} region. The observed spectra were normalized by the IR light power and band frequencies were calibrated by absorption lines of CO_2 and CH_4.

2.2.2 Vacuum Chamber

As schematically shown in Fig. 2.2.2, the vacuum chamber is composed of an ion source chamber and a differentially-pumped ion analyzing chamber, which will be introduced in detail later. A skimmer was set in between the two chambers as an ion-optics component with a tunable voltage. The source chamber was pumped by a turbo molecular pump which was backed up by a mechanic pump. The typical pressure of the chamber without loading the gas was 1.0×10^{-7} Torr, while the working pressure is in the range of 1.0×10^{-5} to 5.0×10^{-5} Torr.

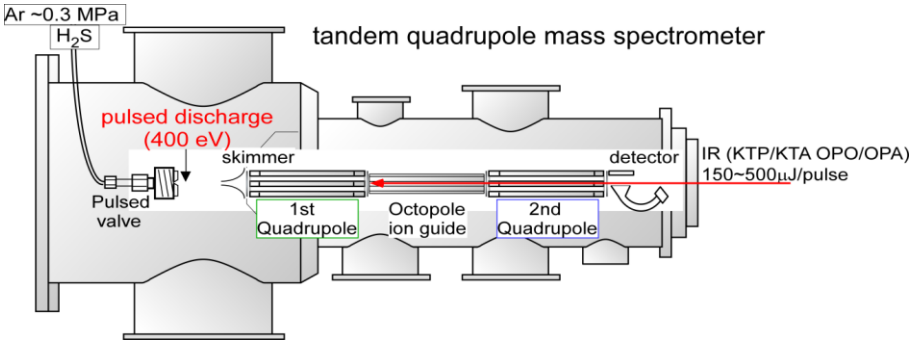

Fig. 2.2.2 Scheme of the vacuum chamber equipped with a tandem quadrupole mass spectrometer used in this study. Reproduced from Ref. 22 with permission from the PCCP Owner Societies.

2.2.3 Ion Source

To produce clusters with low internal energy, a supersonic jet expansion with high pressure is an ideal choice in gas phase studies. This technique overcomes many problems encountered in molecular spectroscopy, such as hot bands, transitions originating from thermally populated vibrational and rotational levels in a large extent. In a supersonic jet expansion, a high pressure gas is expanded from a reservoir into a vacuum through a small orifice.[23,24] The cooling effect in the jet expansion is achieved by the collision of the polyatomic species with the noble gases which have no vibrational or rational modes and exhibit nearly ideal behavior. There are two major steps account for the cooling; in the primary stage of the jet, the velocity of the polyatomic species is accelerated to that of the noble gas, e.g., Argon or Helium, by collision. Subsequently, as the second stage, the relative zero velocity leads to a very low energy collision, thus, the vibrational and rotational temperatures are decreased effectively with only a slight increase in the

translational temperature. Typically, the rotational temperatures could reach in the order of 0.1-10K, through supersonic jet expansion, while, due to the smaller collision cross section for vibrational depopulation, the typical vibrational temperature obtained is around 20-150K. Because of the large excess energy in ionization or protonation, in the case of ionic and protonated species, the temperature tends to be higher.

In the downstream from the orifice, the gas density falls down rapidly, and gradually enters the free-collision region. When ionization occurs at the position close to the nozzle orifice (<1 mm), it allows the ions to cool and participate in clustering reactions with the co-expanding atoms and molecules. In such a region, some of the ionization techniques, such as, discharge, electron ionization, and laser photoionization, can be combined with a supersonic jet expansion to produce ions. Here we chose the combination with discharge to generate ions, which has been frequently used in the previous studies of $H^+(H_2O)_n$. In this method,[25] the gas mixture of H_2S seeded in Ar was expanded into a chamber from a pulsed supersonic valve through a channel nozzle. The channel was equipped with a small pin electrode at its sidewall. The discharge in the channel was triggered by the pulsed high voltage of -400V, which was synchronized with the pulsed valve operation. The protonated cluster cations were cooled on expansion from the channel.

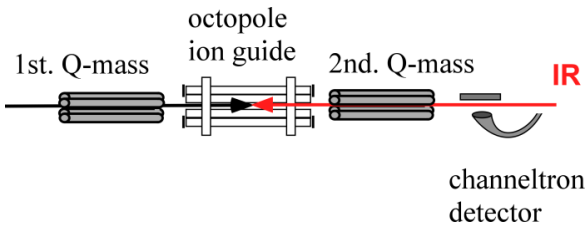

Fig. 2.2.3 Scheme of the tandem quadrupole mass spectrometer

2.2.4 Tandem quadrupole mass spectrometer

Fig. 2.2.3 shows a scheme of the mass spectrometer with two linearly aligned quadrupole mass filters used in this study. The source region of the chamber is evacuated by a turbo molecular pump and separated from the detection region with a skimmer of 3 mm in diameter. Two quadrupoles were connected by an octopole ion guide. In order to achieve high transmission efficiency, we put ion lens at the entrance and exit of each Q-mass and octopole ion guide. Through such assembling, cluster cations of a specific mass to charge ratio, which were size-selected by the front-stage quadrupole mass filters, were introduced into the octopole ion guide. The cluster cations then were irradiated by counter-propagating IR light in the ion guide, and the resulting fragment by vibrational predissociation is mass selected again by the 2^{nd} quadrupole mass filter.

All the voltages of the ion optics, pole bias of each multipole, fine-tuning of mass resolutions, and detector voltages were well controlled by the Merlin controller interface and Merlin automation data system program (Extrel). The ion signal from the channeltron electron multiplier (CEM) detector was amplified by a preamplifier and subsequently sent to the interface. By the processing of Merlin software, a mass spectrum is then available.

2.2.5 IR source

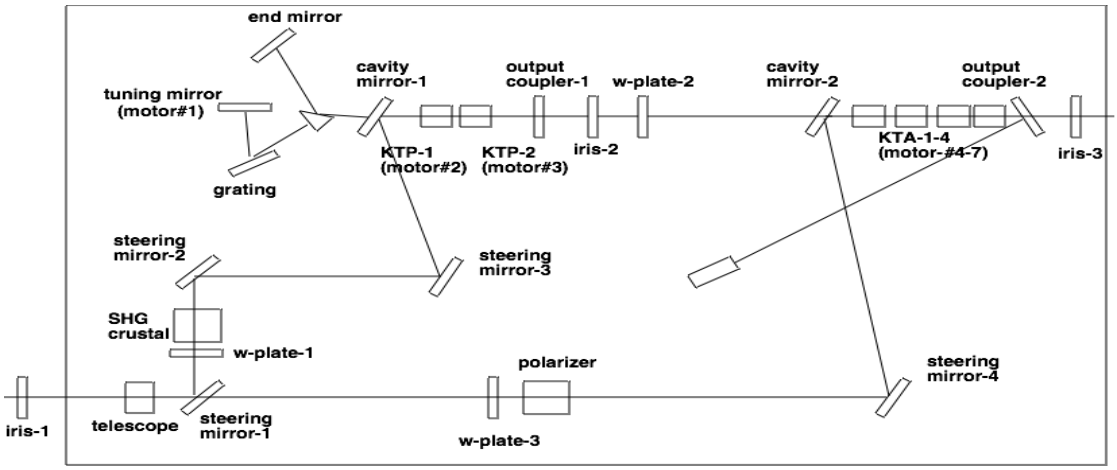

Fig. 2.2.4 Scheme of the IR light source (IR-OPO/OPA).

To produce wide wavelength range IR light in the SH stretch region, we employed a custom-made IR light source (IR-OPO/OPA, LaserVision), which uses the KTP/KTA-based OPO/OPA processes. The process of the tunable IR generation is shown in Fig. 2.2.4. A pump beam, a fundamental output of a Nd:YAG laser (1064 nm, ~560 mJ/pulse), was split into two by a beam-splitter. One of the beams was frequency-doubled with a KTP crystal, giving 532nm light which was used to pump the first OPO stage, which is consisted of two KTP crystals. Then, the combination of the idler output (1345-2122 nm) and the residual light from the pump beam (1064 nm) was introduced to the OPA stage with four KTA crystals. The idler output of the OPA around 2100-4600 cm^{-1} is the IR light we use for measurements. The wavelength tuning of the IR light is performed by tuning the crystal angles via a computer. IR frequency was calibrated by absorption lines of CO_2 and CH_4.

2.3 Calculation

21 calculation levels were adopted to energy-optimize and analyze structures and vibrations of $H^+(H_2S)_3$ with the Eigen type ion-core for evaluation of the calculation method on the present system. Results are summarized in Table 2.3.1. First, the scaling factor for each calculation level was determined by the sym. SH stretch band (ν_1) of the H-bond acceptor H_2S moieties. We fitted the average of the calculated frequencies of the two H-bonded H_2S molecules in $H^+(H_2S)_3$ to the experimental value (2585 cm^{-1}). Then, the calculated frequency of the free SH in H_3S^+ was scaled by this factor, and the resultant frequency was compared with the experimental value (2558 cm^{-1}). The deviation of the calculated value from the experimental one, Δ_{E-C}, is listed in Table 2.3.1. It is seen that the MP2 method shows the good agreement irrespective of the basis sets. Thus, MP2/aug-cc-pVDZ, which has been frequently employed for analyses of neutral SCHB systems,[1] was selected for the level of theory in the following analyses. We also examined the aug-cc-pVTZ basis set, but its combination with MP2 was too much time-consuming for our computational resource. The scaling factor is determined to be 0.945 at the MP2/aug-cc-pVDZ level. Natural bond orbital (NBO) was utilized to analyze the intermolecular interaction. Dissociation energies (D_0) of the clusters were also evaluated with the zero point energy (ZPE) and basis set superposition error (BSSE) correlations. All the computations for the clusters were carried out using the Gaussian09 program package.[26]

Table 2.3.1 Calculated free SH stretch frequencies of $H^+(H_2S)_3$ at different calculation levels. All units are in cm^{-1}.

Calculation level	Stretch of free SH in H_3S^+ [a]	ν_1 in H-bonded H_2S [a],[b]	Scaling factor [c]	Δ_{E-C} [d]
B3LYP/6-311++G(3df,2p)	2659	2674	0.9667	-12
B3LYP/6-311++G(d,p)	2650	2664	0.9703	-13
B3LYP/aug-cc-pVDZ	2675	2696	0.9588	-7
CAM- B3LYP /6-311++G(3df,2p)	2694	2718	0.9511	-4
CAM - B3LYP /6-311++G(d,p)	2689	2714	0.9525	-3
CAM - B3LYP /aug-cc-pVDZ	2675	2697	0.9585	-6
M06-2X/6-311++G(3df,2p)	2700	2745	0.9417	15
M06-2X/6-311++G(d,p)	2688	2740	0.9434	22
M06-2X/aug-cc-pVDZ	2666	2706	0.9553	11
MP2/6-311++G(3df,2p)	2727	2752	0.9393	-3
MP2/6-311++G(d,p)	2773	2806	0.9212	4
MP2/aug-cc-pVDZ	2711	2736	0.9448	-3
MPW1PW91/6-311++G(3df,2p)	N/A	N/A	N/A	N/A
MPW1PW91/6-311++G(d,p)	2694	2707	0.9549	-15
MPW1PW91/aug-cc-pVDZ	2681	2690	0.961	-18
LC-ωPBE/6-311++G(3df,2p)	2755	2781	0.9295	-3
LC-ωPBE /6-311++G(d,p)				
LC-ωPBE /aug-cc-pVDZ	2843	2766	0.9346	-99
ωB97XD/6-311++G(3df,2p)	2734	2754	0.9386	-8
ωB97XD/6-311++G(d,p)	2730	2768	0.9339	8
ωB97XD/aug-cc-pVDZ	2721	2746	0.9414	-4

[a] Values without scaling.

[b] Averaged values between two frequencies of the two acceptor H_2S molecules.

[c] Scaling factors are determined by fitting the observed sym. stretch frequency of free SH in H-bonded H_2S (2585 cm^{-1}) by the corresponding calculated frequency.

[d] Δ_{E-C} is difference between the observed free SH frequency in H_3S^+ (2558 cm^{-1}) and calculated one scaled by the factor determined for the free SH band of the H-bonded H_2S.

2.4 Results and discussion

2.4.1 $H^+(H_2S)_3$ and $H^+(H_2S)_4$

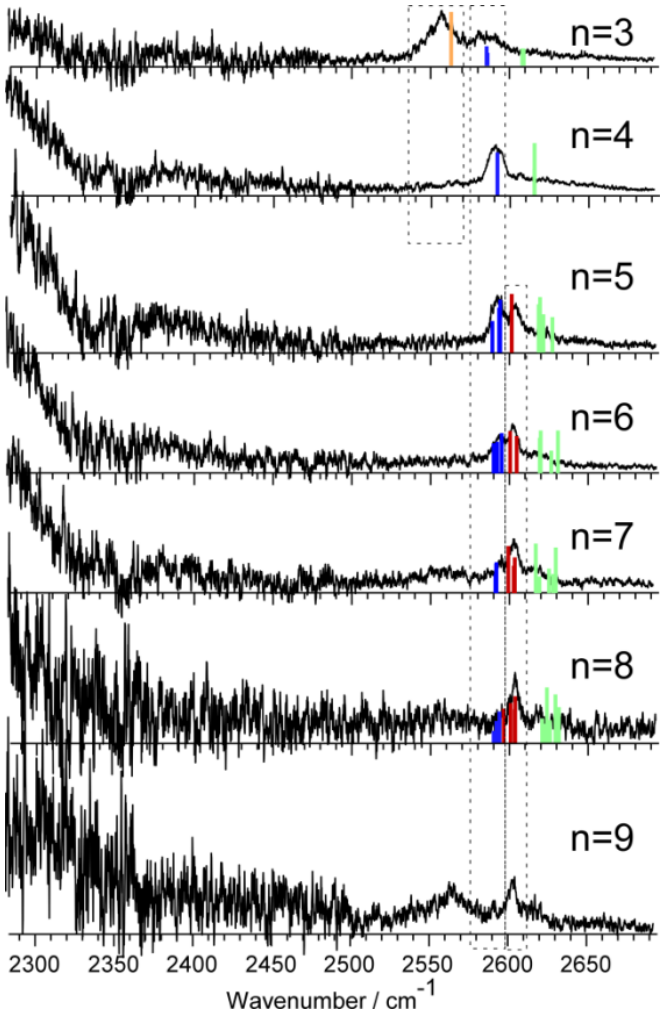

Fig. 2.4.1 Vibrational predissociation spectra of size-selected $H^+(H_2S)_n$ (n = 3 − 9) with their simulated stick spectra based on the most stable energy-optimized structures. The optimized structures for the simulations are shown in Fig. 2.4.2. The harmonic vibration modes are calculated at the MP2/aug-cc-pVDZ level (scaled by 0.945) and are presented as colored sticks. Orange stick: free SH stretch of the Eigen type ion core H_3S^+; Blue sticks: sym. stretch (ν_1) of free SH in H-bonded H_2S; Red sticks: sym. stretch (ν_1) of free SH in charge-dipole bound H_2S; Green sticks: asym. stretch (ν_3) of free SH in both H-bonded and charge-dipole bound H_2S molecules. All the H-bonded SH stretch bands of the ion core are calculated below the observed frequency region (See Table 2.4.1). Reproduced from Ref. 35 with permission from the PCCP Owner Societies.

Table 2.4.1 Calculated SH stretch harmonic vibrational frequencies (in cm^{-1}) of $H^+(H_2S)_n$ (n = 3 – 8) at the MP2/aug-cc-pVDZ level with the scaling factor 0.945. Corresponding optimized structures are shown in Fig. 2.4.2. Frequencies of the observed bands are also shown in parentheses.

	3	**4**	**5-1**	**5-2**	**6**	**7**	**8**	**9**
Stretch of H-bonded SH in H_3S^+	1702 1849	1985[a] 1985[a] 2094	1883 2043 2131	1935 2009 2142	1897 2014 2185	2047 2119 2224	2088 2148 2260	
Stretch of H-bonded SH in neural H_2S								(2564)
Stretch of free SH in H_3S^+	2563 (2558)							
Sym. stretch of free SH in H-bonded H_2S	2585 2586 (2590)	2591[a] 2591[a] 2591[a] (2592)	2589 2593 2594	2591[a] 2591[a] 2593	2590 2593 2595	2590 2591[a] 2591[a]	2590 2591 2593	
			(2593)		(2594)	(2594)		
Sym. stretch of free SH in charge-dipole bound H_2S			2600	2605	2601 2605	2599 2603[a] 2603[a]	2596 2600 2603[a] 2603[a] (2603)	(2603)
			(2605)		(2603)	(2603)		
Asym. stretch of free SH in H-bonded H_2S	2609 2610	2614[a] 2614[a] 2614[a]	2618 2619 2621	2616 2618 2619	2619[a] 2619[a] 2620	2616 2618 2619	2620 2621 2623	
Asym. stretch of free SH in charge-dipole bound H_2S			2627	2631	2627 2630	2625 2627 2629	2622 2625 2629 2631	

[a] Degenerated frequencies

IR predissociation spectra of size-selected $H^+(H_2S)n$ (n = 3 − 9) obtained by monitoring the single H_2S loss channel are displayed in Fig. 2.4.1 with the simulated stick spectra at the MP2/aug-cc-pVDZ level. The energy-optimized structures corresponding to the spectral simulations are shown in Fig. 2.4.2. All the frequencies and assignments of the observed bands are summarized in Table 2.4.1.

In the observed spectrum of n = 3, three features are seen; intense and broadened absorption below ca. 2400 cm^{-1} and two relatively sharp bands at 2558 and 2585 cm^{-1}. The broadened absorption is obviously attributed to the tail of strong H-bonded SH stretch bands of the protonated ion core. Its peak is expected to be lower than 2300 cm^{-1}, which is the low frequency limit of the reliable measurement by the present experiment system. Extremely broadened absorption of such an ion core vibration has also been reported for $H^+(H_2O)_3$.[4,5] The sharp band at 2558 cm^{-1} in the spectrum of n = 3 suddenly disappears in $n \geq 4$. The absence of the band for $n \geq 4$ gives unambiguous implication that this band is attributed to the free SH stretch of the ion core, and the ion core is the Eigen type, H_3S^+. This is because the first H-bonded solvation shell of the Eigen type ion core should be completed at n = 4. This spectral assignment is also supported by the good agreement with the simulated spectra based on the minimum energy structures (details will be discussed below). Therefore, the development of the proton solvation structure in $H^+(H_2S)_n$ is parallel to that in $H^+(H_2O)_n$ at n = 3 and 4.[4,5] In the structures of n = 3 and 4, free SH should exist in the neutral moiety (H-bonded shell) and the observed bands at 2585 and 2590 cm^{-1}, respectively, are uniquely assigned to their stretch vibration (symmetric stretch, ν_1). Free SH stretch bands of neutral H_2S monomer (ν_1 and asym. stretch ν_3) have been reported at

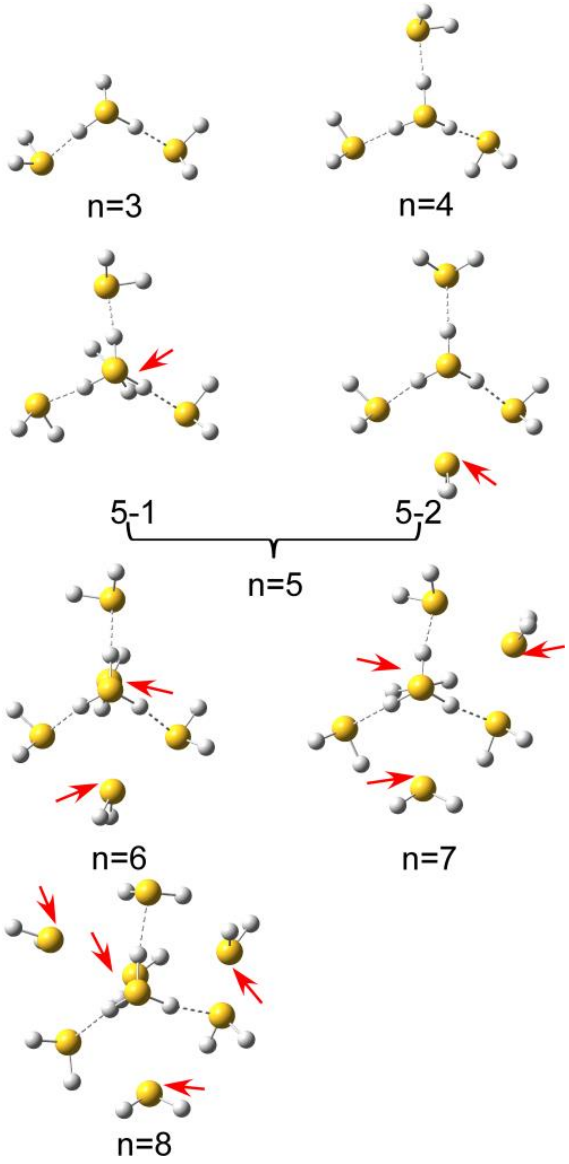

Fig. 2.4.2 Energy-optimized structures of $H^+(H_2S)_n$ (n = 3 − 8) identified by the observed spectra. H_2S molecules bound by the charge-dipole interaction are denoted by red arrows. The spectral simulations in Fig. 2.4.1 are based on these structures (for n = 5, more stable structure **5-1** is used). Energy optimization of the structures was performed at the MP2/aug-cc-pVDZ level. Reproduced from Ref. 35 with permission from the PCCP Owner Societies.

2614 and 2628 cm^{-1}, respectively,[27] and the small low-frequency shifts are attributed to the influence of the excess charge in the ion core. Absence of a clear ν_3 band in the observed spectra will be discussed later.

2.4.2 $H^+(H_2S)_5$

As seen in the spectrum of n = 5 in Fig. 2.4.1, a new free SH band strongly appears at 2605 cm^{-1}. If the second H-bonded shell begins to form following the completion of the first shell at n = 4, an H-bonded SH band of the neutral moiety (H-bonded SH of the first shell molecule) is expected in the frequency region lower than the free SH band (< 2585 cm^{-1}) However, such a band is totally absent. This suggests that the second H-bonded shell is not formed in n = 5 and the solvation structure is quite different from that of $H^+(H_2O)_5$, in which the fifth H_2O interacts only with the first solvation shell by an H-bond.[3,4,6,28]

To uncover the structure of $H^+(H_2S)_5$, we turn to quantum chemical calculations at the MP2/aug-cc-pVDZ level. Fig. 2.4.3 shows the comparison between the harmonic simulated spectra of stable isomer structures and the experimental spectrum. Because the H-bonded SH stretch bands of the ion core are largely red-shifted beyond the measured frequency range, thus their frequencies are not given in Fig. 2.4.3, but they are found in Table 2.4.2.

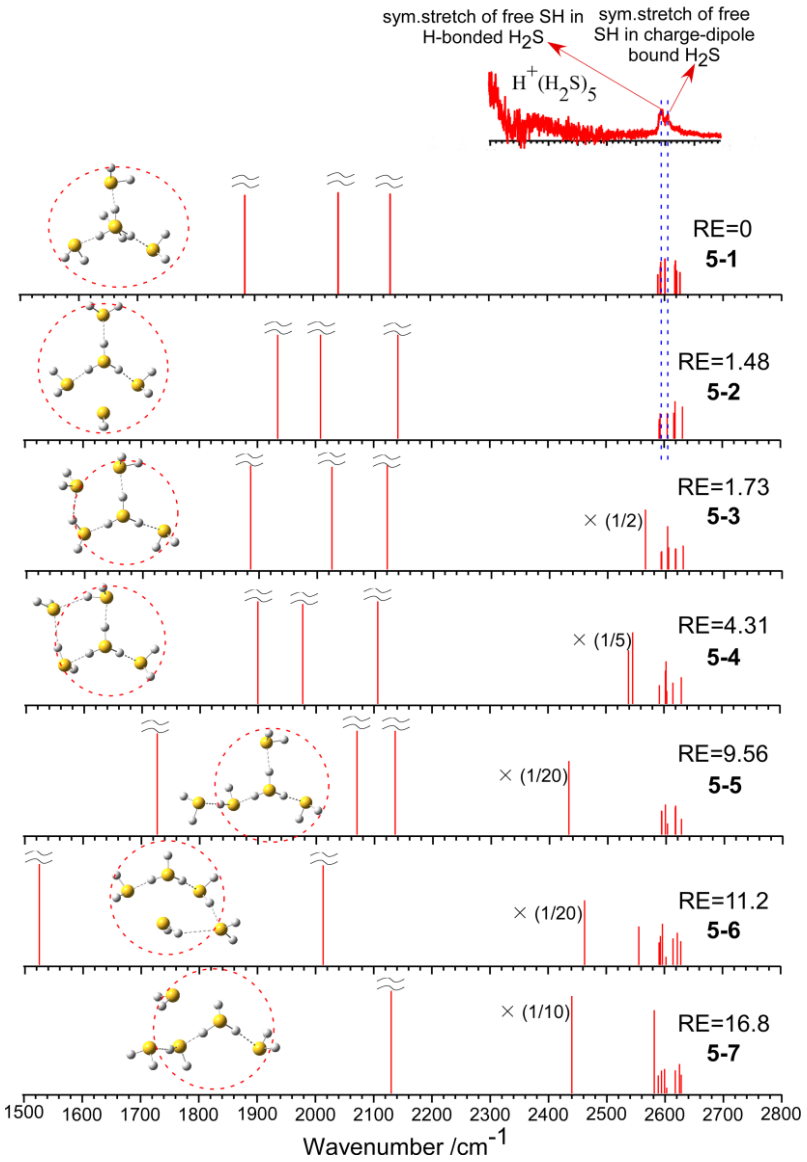

Fig. 2.4.3 Comparison between the experimental and simulated IR spectra of $H^+(H_2S)_5$. The simulation was performed at the MP2/aug-cc-pVDZ level with the scaling factor 0.945. Relative energies (RE) are in kJ/mol. Red dotted circles indicate the first solvation shell. Note that the structures with the second H-bonded shell formation (**5-3** to **5-7**) show H-bonded SH stretch bands of the neutral H_2S moiety (their intensities are scaled in the spectra), but the observed spectrum lacks a corresponding band. Reproduced from Ref. 35 with permission from the PCCP Owner Societies.

Table 2.4.2 Calculated SH stretch harmonic vibrational frequencies (in cm^{-1}) and their assignments of all the isomers of $H^+(H_2S)_5$ shown in Fig. 2.4.3. The calculation level is MP2/aug-cc-pVDZ and the scaling factor of 0.945 is applied.

	5-1	**5-2**	**5-3**	**5-4**	**5-5**	**5-6**	**5-7**
Stretch of H-bonded SH in H_3S^+	1883 2043 2131	1935 2009 2142	1886 2026 2121	1900 1977 2106	1727 2070 2135	1525 2013	1323 2130
Stretch of H-bonded SH in neutral H_2S			2565	2539 2546	2433	2463	2440
Stretch of free SH in H_3S^+						2556	2581
Sym. stretch of free SH in H-bonded H_2S	2589(1st shell)[a] 2593(1st shell) 2594(1st shell	2591(1^{st} shell) 2591(1^{st} shell) 2593(1^{st} shell)	2592(1^{st} shell) 2593(1^{st} shell) 2603(2^{nd} shell)[b] 2605(2^{nd} shell)[b]	2592(1^{st} shell) 2603(2^{nd} shell)[b] 2604(2^{nd} shell)[b] 2605(2^{nd} shell)[b]	2592(1^{st} shell) 2593(1^{st} shell) 2602(2^{nd} shell)	2591(1^{st} shell) 2603(2^{nd} shell)	2594(1^{st} shell) 2603(2^{nd} shell)
Stretch of free SH in the 1^{st} shell H-bonded H_2S			2603[b] 2605[b]	2603[b] 2604[b] 2605[b]	2599	2593	2588

Sym. stretch of free SH in charge-dipole bound H_2S	2600	2605				2597	2599
Asym. stretch of free SH in H-bonded H_2S	2618(1^{st} shell) 2619(1^{st} shell) 2621(1^{st} shell)	2616(1^{st} shell) 2618(1^{st} shell) 2619(1^{st} shell)	2617(1^{st} shell) 2630(2^{nd} shell)	2616(1^{st} shell) 2630(2^{nd} shell)	2616(1^{st} shell) 2616(1^{st} shell) 2626(2^{nd} shell)	2615(1^{st} shell) 2628(2^{nd} shell)	2617(1^{st} shell) 2628(2^{nd} shell)
Asym. stretch of free SH in charge-dipole bound H_2S	2627	2631				2622	2625

[a] The H_2S molecules in the "1^{st} shell" are highlighted by the dotted red circle in Fig. 2.4.3 in the main text while the molecules outside the circle belong to the "2^{nd} shell".

[b] The stretch frequency of free SH in the 1^{st} shell H-bonded H_2S is mixed with the sym. stretch of free SH in 2^{nd} shell H-bonded H_2S for isomer **5-3**. Therefore, for these two types of stretch, only single band exists for each. This case is the same for structure **5-4**.

The structural search demonstrates that in n = 5, after the completion of the first H-bonded shell, the fifth H_2S still prefers directly solvating the ion core (**5-1** and **5-2**) rather than the second H-bonded solvation shell formation (**5-3** to **5-7**). The fifth H_2S can locate either under the umbrella of the H_3S^+ moiety (**5-1**) or in the same plane as the H-bonded shell molecules (**5-2**). The sulfur atom of the fifth H_2S faces to the ion core, and these structures indicate that the charge-dipole interaction would be the major component of the intermolecular interactions. Both the charge-dipole shell structures are estimated to be more stable than second H-bonded shell structures. Second H-bonded shell structure is higher in energy by at least 1.73 kJ/mol than most stable structure **5-1**. As seen in Fig. 2.4.3, the structures with the second H-bonded shell formation show H-bonded SH stretch bands of the neutral H_2S moiety below 2580 cm^{-1} (note that their intensities are scaled in the simulated spectra), but the observed spectrum totally lacks such a band. Therefore, the observed spectrum should be exclusively carried by the charge-dipole shell structures. At n = 5, two possible sites for the charge-dipole shell are energetically almost degenerated (structure **5-2** is +1.48 kJ/mol to structure **5-1,** with the ZPE correction). As shown in later, the energy evaluation may be influenced by the BSSE correction. Moreover, the relative population of isomers would change with temperature. Therefore, at the present stage, we suppose both structures **5-1** and **5-2** contribute to the observed spectrum. Structure **5-1**, the most stable isomer, is temporally chosen for the spectral simulation in Fig. 2.4.1. The spectral simulation based on the charge-dipole shell structure explains well the absence of the H-bonded SH band of the neutral moiety in the observed spectra, and the band at 2605 cm^{-1} is attributed to the ν_1 of free SH of H_2S in the charge-dipole shell. Only the second H-

bonded shell structure similar to $H^+(H_2O)_n$ has been calculated for $H^+(H_2S)_n$ so far.[21] The charge-dipole shell formation following the first H-bonded shell completion is demonstrated for the first time in the present work.

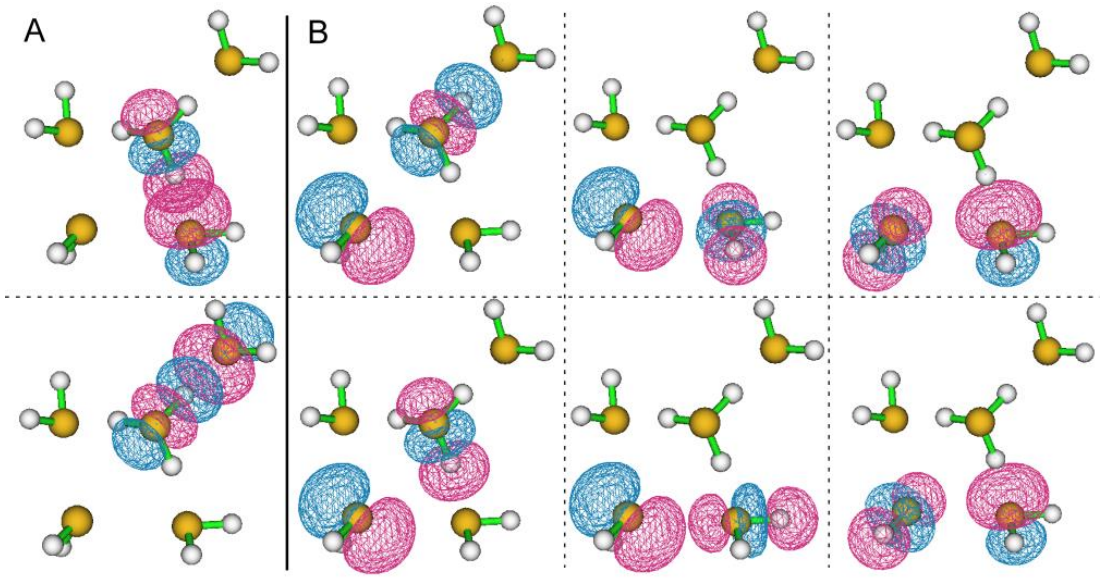

Fig. 2.4.4 The natural bond orbitals of $H^+(H_2S)_5$ (isovalue=0.006). In panel A, the lone pair orbital (n) of H-bonded H_2S and the antibonding orbital (σ*) of S-H in the H_3S^+ ion-core exhibits an apparent overlap, indicating a hydrogen bond. In panel B, any kind of overlap between the lone pair orbital (n) and the antibonding orbital (σ*) is absent in the charge-dipole shell. Reproduced from Ref. 35 with permission from the PCCP Owner Societies.

To obtain more insight into the interactions involved in the intermolecular structures, the NBO analysis is adopted, as it provides a quantitative assessment of an H-bond in terms of donor-acceptor charge delocalization by the second-order perturbation theory. As seen in panel A of Fig. 2.4.4 for $H^+(H_2S)_5$ (for clarity of viewing, only structure **5-2** is selected), an H-bond is stabilized by charge (electron) transfer from an S lone pair (n) orbital of H-bonded H_2S to the proximal S-H antibonding (σ^*) orbital of the H_3S^+ core, with the stabilization energy E(2) for three H-bonds, 45.9, 45.8, and 34.0 kcal/mol, respectively (the H-bonds proximal to the charge-dipole shell molecule correspond to the larger two values). On the other hand, as seen in panel B of Fig. 2.4.4, any kind of overlap between the occupied and adjacent virtual orbitals is not observed between the charge-dipole shell molecule and the neighboring molecules. This analysis explicitly leads to the non-hydrogen-bonding character of the charge-dipole shell.

One may note that both in the H-bonded and charge-dipole shells, only the ν_1 band strongly appears and the ν_3 band is much weaker or almost disappears in the observed spectra. The similar trend has been frequently observed for H_2O directly solvating a protonated or positively charged site.[29,30] Three reasons could be supposed to account for the weak ν_3 band. (i) The ν_1 intensity should be largely enhanced in such a system as its transition dipole moment is parallel to the electric field of the ion core while that of the ν_3 band is perpendicular to the field.[29] (ii) The ν_3 band shows a wider hindered rotation structure due to P and R branches while that of the ν_1 mode is sharper due to a Q branch.[30,31] (iii) The lower dissociation rate (yield) in the ν_3 mode excitation can be caused by the weak coupling between ν_3 and the intermolecular stretch mode.[30]

2.4.3 $H^+(H_2S)_6$ to $H^+(H_2S)_9$

In the size range of $n = 5 - 8$, the basic spectral motifs are kept, as shown in Fig. 2.4.1, but a remarkable intensity ratio change happens between the two free SH bands of neutral H_2S with increasing of the cluster size. The intensity of the H-bonded shell band is gradually overtaken by the charge-dipole shell band. This spectral change clearly exhibits the filling process of the charge-dipole shell. To support this interpretation, stable isomer structures were searched for $H^+(H_2S)_6$ and $H^+(H_2S)_7$, and the results are summarized in Figs. 2.4.5 and 2.4.6, respectively. More information is available in Tables 2.4.3 and 2.4.4. The structural search was performed by manual construction of the initial structures, which are inferred from the structures of $H^+(H_2S)_5$. Since there would be a large number of possible structures in $n = 6$ and 7, we do not exclude the possibility of low-lying structures other than those shown in the figures. Search for $H^+(H_2S)_8$ was not performed because of its practical difficulty and computational cost. In the present search results, similar to $H^+(H_2S)_5$, the charge-dipole shell structures are the most stable isomers in both the sizes. In the charge-dipole shell, however, H_2S clearly prefers locating under the umbrella (out-of-plane) rather than in the plane of the ion core (in-plane). The energy difference between these two solvation sites increases from 1.48 kJ/mol for $H^+(H_2S)_5$ (between **5-1** and **5-2**) to 5.36 kJ/mol for $H^+(H_2S)_6$ (between **6-1** and **6-2**) and 6.58 kJ/mol for $H^+(H_2S)_7$ (between **7-1** and **7-6**). It is also seen that energy separation between the in-plane type charge-dipole shell structures and second H-bonded shell structures decreases with increasing size (e.g., **5-2** and **5-5**, **6-2** and **6-5**), and some of the second H-bonded shell structures (e.g**., 7-5**) become more stable than the in-plane type charge-dipole shell structures in $n = 7$ (**7-7**). However,

the observed spectra definitely demonstrate that the charge-dipole shell is superior to the second H-bonded shell up to n = 8, because the H-bonded SH bands of the first shell molecules, which are expected below 2580 cm^{-1} with a large intensity, are undoubtedly absent. At n = 9, a somewhat broadened band finally appears at 2564 cm^{-1}. The frequency of this band coincides well with the SH stretch band of crystalline H_2S,[32] and the band is assigned to an H-bonded SH stretch of the neutral moiety. Therefore, this band indicates the beginning of the second H-bonded shell formation.

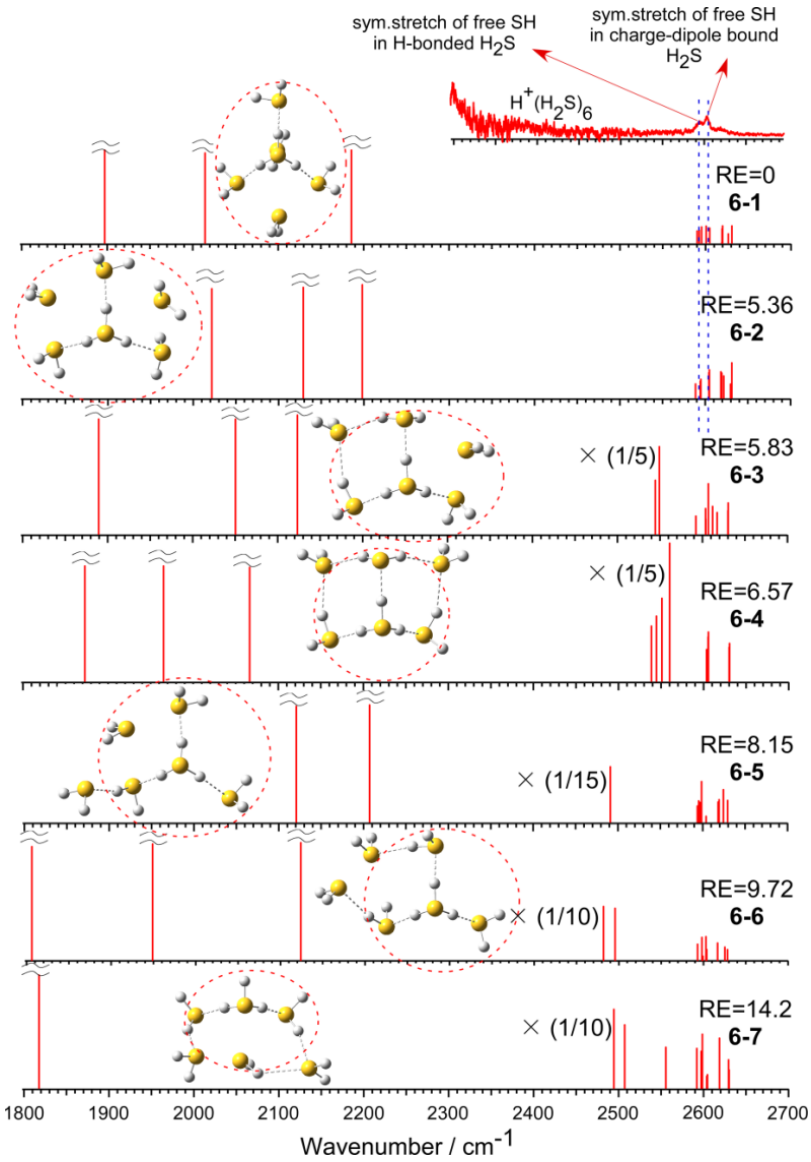

Fig. 2.4.5 Comparison between the experimental and simulated IR spectra of $H^+(H_2S)_6$. The simulation was performed at the MP2/aug-cc-pVDZ level with the scaling factor 0.945. Relative energies (RE) are in kJ/mol. Red dotted circles indicate the first solvation shell. Note that the structures with the second H-bonded shell formation (**6-3** to **6-7**) show H-bonded SH stretch bands of the neutral H_2S moiety (their intensities are scaled in the simulated spectra), but the observed spectrum lacks a corresponding band. Reproduced from Ref. 35 with permission from the PCCP Owner Societies.

Table 2.4.3 Calculated SH stretch harmonic vibrational frequencies (in cm^{-1}) and their assignments of all the isomers of $H^+(H_2S)_6$ shown in Fig. 2.4.5. The calculation level is MP2/aug-cc-pVDZ and the scaling factor of 0.945 is applied.

	6-1	**6-2**	**6-3**	**6-4**	**6-5**	**6-6**	**6-7**
Stretch of H-bonded SH in H_3S^+	1897 2014 2185	2022 2129 2198	1890 2050 2123	1873 1965 2066	1785 2121 2207	1806 1949 2124	1655 1818
Stretch of H-bonded SH in neutral H_2S			2544 2549	2544 2551	2491	2482 2496	2494 2507
Stretch of free SH in H_3S^+							2556
Sym. stretch of free SH in H-bonded H_2S	2590(1^{st} shell) 2593(1^{st} shell) 2595(1^{st} shell)	2589(1^{st} shell) 2594(1^{st} shell) 2595(1^{st} shell)	2592(1^{st} shell) 2604(2^{nd} shell)	2603(2^{nd} shell) 2604(2^{nd} shell)	2594(1^{st} shell) 2595(1^{st} shell) 2604(2^{nd} shell)	2593(1^{st} shell) 2598(2^{nd} shell)[a] 2599(2^{nd} shell)[a] 2604(2^{nd} shell)	2604(2^{nd} shell) 2605(2^{nd} shell)
Stretch of free SH in the 1^{st} shell H-bonded H_2S			2607 2612	2605 2606	2597	2598[a] 2599[a] 2603	2597 2599

Sym. stretch of free SH in charge-dipole bound H_2S	2601 2605	2604 2605	2604		2599		2592
Asym. stretch of free SH in H-bonded H_2S	2619(1^{st} shell) 2619(1^{st} shell) 2620(1^{st} shell)	2618(1^{st} shell) 2619(1^{st} shell) 2622(1^{st} shell)	2617(1^{st} shell) 2630(2^{nd} shell)	2630(2^{nd} shell)	2618(1^{st} shell) 2619(1^{st} shell) 2629(2^{nd} shell)	2617(1^{st} shell) 2625(2^{nd} shell) 2628(2^{nd} shell)	2629(2^{nd} shell) 2630(2^{nd} shell)
Asym. stretch of free SH in charge-dipole bound H_2S	2627 2630	2630 2631	2630		2624		2619

[a] The stretch frequency of free SH in the 1^{st} shell H-bonded H_2S is mixed with the sym. stretch of free SH in 2^{nd} shell H-bonded H_2S for isomer **6-6**. Therefore, for these two types of stretch, only single band exists for each.

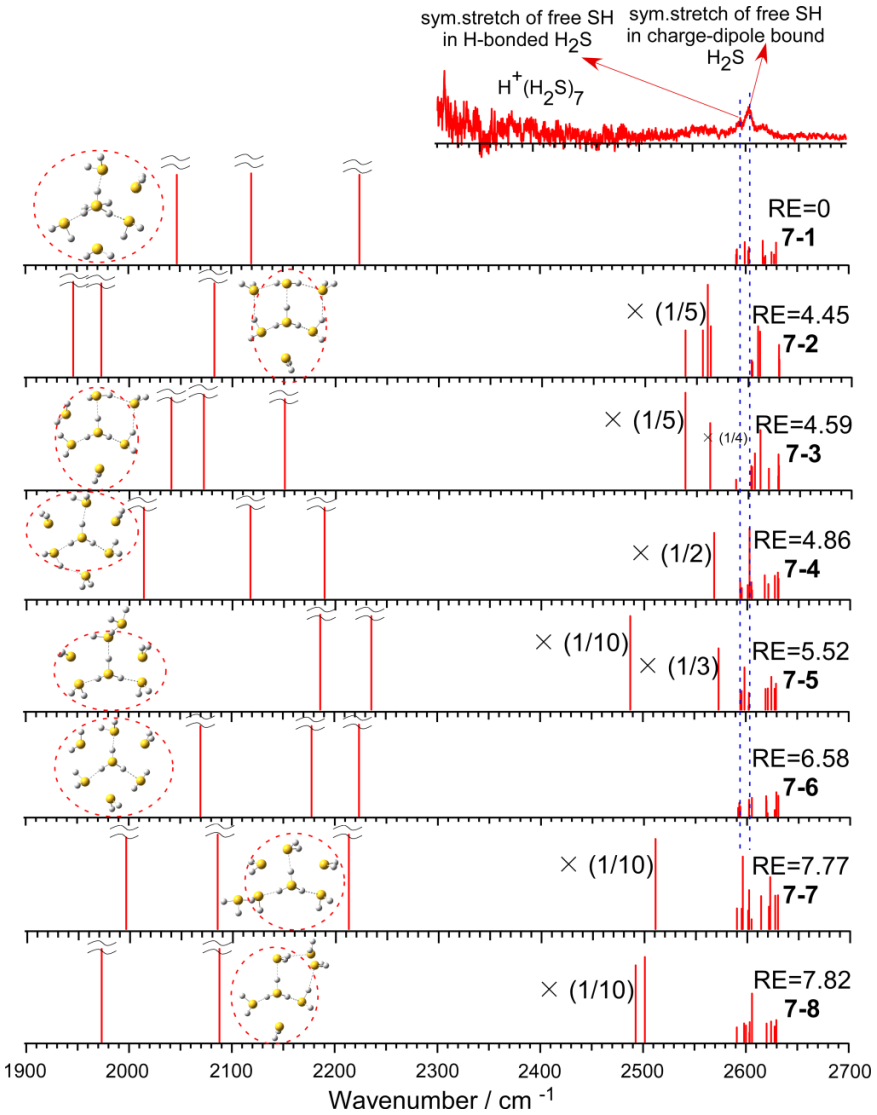

Fig. 2.4.6 Comparison between the experimental and simulated IR spectra of $H^+(H_2S)_7$. The simulation was performed at the MP2/aug-cc-pVDZ level with the scaling factor 0.945. Relative energies (RE) are in kJ/mol. Red dotted circles indicate the first solvation shell. Note that the structures with the second H-bonded shell formation (**7-2** to **7-5**, **7-7** and **7-8**) show H-bonded SH stretch bands of the neutral H_2S moiety (their intensities are scaled in the simulated spectra), but the observed spectrum lacks a corresponding band. Reproduced from Ref. 35 with permission from the PCCP Owner Societies.

Table 2.4.4 Calculated SH stretch harmonic vibrational frequencies (in cm^{-1}) and their assignments of all the isomers of $H^+(H_2S)_7$ shown in Fig. 2.4.6. The calculation level is MP2/aug-cc-pVDZ and the scaling factor of 0.945 is applied.

	7-1	**7-2**	**7-3**	**7-4**	**7-5**	**7-6**	**7-7**	**7-8**
A[b]	2047 2119 2224	1946 1973 2082	2041 2072 2151	2014 2117 2189	1607 2186 2236	2069 2177 2223	1996 2085 2213	1897 1973 2088
B[c]		2539 2556 2560 2563	2539 2563	2568	2487		2511	2493 2501 2600
C[d]	2590(1^{st} shell) 2591(1^{st} shell) 2591(1^{st} shell)	2588(1^{st} shell) 2603(2^{nd} shell)	2603(2^{nd} shell) 2604(2^{nd} shell)	2593(1^{st} shell) 2595(1^{st} shell) 2602(2^{nd} shell)[a] 2604(2^{nd} shell)[a]	2595(1^{st} shell) 2596(1^{st} shell) 2603(2^{nd} shell)	2591(1^{st} shell) 2592(1^{st} shell) 2593(1^{st} shell)	2590(1^{st} shell) 2594(1^{st} shell) 2604(2^{nd} shell)	2591(1^{st} shell) 2598(2^{nd} shell) 2603(2^{nd} shell)
D[e]		2609 2611	2606 2611	2602[a] 2604[a]	2573		2602	2606
E[f]	2599 2603 2603	2604	2603 2604	2600 2605	2598 2603	2602 2605 2605	2596 2601	2604

F[g]	2616(1^{st} shell) 2618(1^{st} shell) 2619(1^{st} shell)	2629(2^{nd} shell) 2630(2^{nd} shell)	2620(1^{st} shell) 2629(2^{nd} shell)	2617(1^{st} shell) 2620(1^{st} shell) 2630(2^{nd} shell)	2619(1^{st} shell) 2621(1^{st} shell) 2628(2^{nd} shell)	2618 2619 2620	2613(1^{st} shell) 2621(1^{st} shell) 2630(2^{nd} shell)	2620(1^{st} shell) 2624(2^{nd} shell) 2628(2^{nd} shell)
G[h]	2625 2627 2629	2630	2629 2630	2626 2630	2625 2629	2627 2628 2630	2622 2627	2630

[a] The stretch frequency of free SH in the 1^{st} shell H-bonded H_2S is mixed with the sym. stretch of free SH in 2^{nd} shell H-bonded H_2S for isomer **7-4**. Therefore, for these two types of stretch, only single band exists for each.

[b] Stretch of H-bonded SH in H_3S^+.

[c] Stretch of H-bonded SH in neutral H_2S.

[d] Sym. stretch of free SH in H-bonded H_2S.

[e] Stretch of free SH in the 1^{st} shell H-bonded H_2S.

[f] Sym. stretch of free SH in charge-dipole bound H_2S.

[g] Asym. stretch of free SH in H-bonded H_2S

[h] Asym. stretch of free SH in charge-dipole bound H_2S.

2.4.4 Dissociation energy, maximum temperature, and Gibbs energy

Dissociation energies (D_0) for the structures in Fig. 2.4.2 (the most energetically favorable structure at each size) are given in Table 2.4.5. For n = 6 – 8, two dissociation channels, loss of the out-of-plane H_2S and in-plane H_2S in the charge-dipole shell, are possible, and both the channels are calculated. Because of the presence of the heavy atoms (S atoms) in the system, the size of the BSSE correction is large. For n = 5, the order of the dissociation energies of isomers **5-1** and **5-2** is reversed with the BSSE corrections due to the small energy difference between the two isomers. This result suggests optimization with a larger basis set or that with BSSE corrections would be requested to definitely determine the energy order of isomers. At the present stage, these two dissociation paths are regarded to be essentially same in energy. The same phenomenon occurs also in the two dissociation channels of **6-1**. The magnitude of the H-bond in $H^+(H_2S)_n$ is approximately half of that of $H^+(H_2O)_n$ (for example, D_0 of $H^+(H_2O)_4$ is 83.3 kJ/mol at the ωB97X-D/6-311++G(3df,2p) level[6]). With increasing cluster size, the dissociation energy in the charge-dipole shell is clearly lowered. This is probably due to the delocalization of the excess charge in the ion core H_3S^+. The magnitude of the dissociation (binding) energy in the charge-dipole shell is at the border between weak and moderate hydrogen bonds in typical neutral systems.[33]

Table 2.4.5 Dissociation energy (D_0) and maximum temperature (T_{max}) of selected isomers of $H^+(H_2S)_n$. The ZPE corrections are included. All units are kJ/mol, except T_{max} in K.

	D_0 (without BSSE)	BSSE correction	D_0 (with BSSE)	Dissociation channel	Frag.[a]	T_{max}
3	56.8	9.47	47.3			575
4	51.2	8.87	42.3			395
5-1	32.3	10.9	21.3	Loss of out-of-plane H_2S	**4**	204
5-2	30.8	8.50	22.3	Loss of in-plane H_2S	**4**	
6-1	30.3	8.76	21.5	Loss of in-plane H_2S	**5-1**	
	31.8	11.1	20.6	Loss of out-of-plane H_2S	**5-2**	170
7-1	26.3	8.85	17.4	Loss of in-plane H_2S	**6-1**	
	31.6	11.5	20.1	Loss of out-of-plane H_2S	**6-2**	140
8	25.3	9.01	16.2	Loss of in-plane H_2S	**7-1**	
	31.8	13.0	18.9	Loss of out-of-plane H_2S	**7-6**	119

[a] Isomer structure of the charged fragment in the dissociation channel.

Maximum temperature (T_{max}) of the clusters is also evaluated from the dissociation energy and is displayed in Table 2.4.5. T_{max} is the temperature at which the thermal vibrational energy (E_{vib}) is equal to the dissociation energy. We suppose that the cluster can survive at temperature lower than T_{max}, otherwise it should dissociate before the measurement. Herein, E_{vib} was evaluated under the harmonic oscillator approximation.[34] As seen in Table 2.4.5, T_{max} falls with increasing cluster size, reflecting the lowering of the dissociation energy, and T_{max} of the clusters of $n > 4$ are lower than *ca.* 200 K. Therefore, though the harmonic approximation is a crude approximation, it seems reasonable to

assume that the temperature of the observed $H^+(H_2S)_n$ clusters of $n > 4$ is equal or lower than *ca.* 200 K.

To estimate the temperature dependence of the isomer population, we evaluated the Gibbs free energy of the isomers of $n = 5$ up to 200 K. The results are summarized in Table 2.4.6. As seen in Table 2.4.6, the isomer with the lowest Gibbs energy changes between the charge-dipole type structures, **5-1** and **5-2**, with temperature, indicating the change of the dominant isomer in the population. At the present stage, we have no experimental data to evaluate the temperature of the observed cluster, and it is difficult to unambiguously determine the observed isomer. We also should note that the Gibbs energies of the second H-bonded shell type structures are higher than (at least one of) those of the charge-dipole type structures throughout the temperature range, and this is consistent with the lack of the spectral signature of the second H-bonded shell type structures in the observed spectrum.

Table 2.4.6 Gibbs energies at different temperatures for the isomers of $H^+(H_2S)_5$**.** All units are in kJ/mol. Calculations were performed at MP2/aug-cc-pVDZ.

	50 K	100 K	150 K	200 K
5-1	0	1.74	3.93	6.17
5-2	0.286	0	0	0
5-3	1.08	1.64	2.54	3.46
5-4	3.36	3.73	4.57	5.49
5-5	7.40	5.93	4.88	3.92
5-6	11.0	12.2	13.8	15.4
5-7	16.0	16.2	16.6	17.1

4.5 Overview of the structures

The overview of the solvation structure evolution of $H^+(H_2S)_n$ till the first solvation shell completion is illustrated in Fig. 2.4.2. In addition to the three H-bond solvation sites, there are four sites for the charge-dipole solvation of the ion core; three of them are in the plane of the first H-bonded shell, and remaining one is under the umbrella of the ion core. Totally seven H_2S molecules can directly solvate the ion core. Regarding the four sites of the charge-dipole shell, the present MP2/aug-cc-pVDZ calculations suggest the first preference of the site under the umbrella of H_3S^+. However, these four sites are not distinguishable from the observed spectra. Calculations at higher levels (e.g., the aug-cc-pVTZ basis set and optimization with BSSE corrections) are requested for the definite conclusion of the preferential site in the charge-dipole shell. Temperature (internal energy) control of the clusters by a cryogenic ion trap or inert gas tagging is a future experimental task to obtain more firm information on the (free) energy order of the isomer structures. Under the present experimental condition, we observed the beginning of the second H-bonded shell formation at $n = 9$. However, because the larger flexibility is expected for the second H-bonded shell, its formation may be more competitive at higher temperature.

The preference of the charge-dipole shell formation over the second H-bonded shell is a quite unique property of $H^+(H_2S)_n$. The magnitude of the H-bonds between the ion core and the first shell is largely enhanced by the excess charge of the core, relative to the H-bonds between the first and second H-bonded shells which are those between essentially neutral molecules. Meanwhile, the magnitude of H-bonds between neutral H_2S molecules is

Table 2.4.7 Relative energies among the optimized structures of $H^+(H_2S)_5$ by various calculation methods. All units are in kJ/mol.

	5-5	**5-2**	**5-1**
with dispersion correction			
MP2/aug-cc-pVDZ	9.56	1.48	0
M062x/aug-cc-pVDZ	20.5	8.72	0
M062X/6-311++G(3df,2p)	12.3	0.436	0
M062x/6-311++g(d,p)	17.5	8.39	0
ωB97xD/aug-cc-pVDZ	3.85	0.971	0
ωB97XD/6-311++G(3df,2p)	2.81	0	1.26
ωB97XD/6-311++g(d,p)	5.47	0	0.683
without dispersion correction			
B3LYP/aug-cc-pVDZ	0	3.58	N/A
B3LYP/6-311++G(3df,2p)	2.66	0	N/A
B3LYP/6-311++G(d,p)	0	N/A	N/A

much smaller than those of H_2O molecules. Thus, the charge-dipole interaction with the ion core can be superior to the H-bond between the first and second shells. It is noteworthy that a large induced dipole moment is expected for H_2S in the charged system because of its large polarizability (see Table 2.1.1). To form such a dense solvation structure around the ion core, not only the charge-dipole interaction but also dispersion should play an important role.[9-13] This is because dispersion can contribute to the attraction with all neighboring

molecules and it becomes more effective in a denser structure. This interpretation is simply proved by the fact that B3LYP level calculations, which are known to lack the contribution of dispersion, largely underestimate the stability of the charge-dipole solvation structures relative to the second H-bonded shell structures. In contrast, dispersion-corrected DFT calculations show similar trend with the MP2 results. The details are provided in Table 2.4.7. For more quantitative description of the contribution of dispersion, an energy decomposition analysis is needed.

Finally, we briefly comment on some implications of the present results for H-bonded structures of $H^+(H_2O)_n$. Though H_2S has the same H-bond coordination property with H_2O, the proton solvation structures following the first H-bonded solvation shell are totally different between these two systems. Because of the small magnitude of H-bonds in $H^+(H_2S)_n$, the charge-dipole shell formation is superior to the second H-bonded shell formation. Such charge-dipole shell formation has never been found in $H^+(H_2O)_n$, and H-bonds are an exclusive factor in construction of intermolecular structures of $H^+(H_2O)_n$. The present finding shows that there should be a threshold of H-bond strength to keep its exclusive role in intermolecular structure construction. In addition, no sign of Zundel type ion-core structures was obtained for $H^+(H_2S)_n$ of $3 \leq n \leq 9$ while the competition between the Eigen and Zundel type isomers has been revealed in $H^+(H_2O)_n$, especially at $n = 6$.[6] The competition between the Eigen and Zundel ion-cores is the key concept of the Grotthhus mechanism of proton transfer. In the present study, no IR dissociation signal could be detected for $H^+(H_2S)_2$ because of its high dissociation energy, and its ion core motif was not determined. However, collapse of the Zundel ion core in $H^+(H_2S)_6$ is clearly concluded

from the observed spectrum, and this is in contrast with the fact that the Zundel type isomer is the global minimum in $H^+(H_2O)_6$. Thus, the present result suggests that the Zundel type ion-core is not stable in weak H-bonded systems, at least for an H-bonded solvation shell. These findings imply that not only the coordination property but also the magnitude of the interaction is highly important to determine intermolecular structures.

2. 5. Conclusions

The structures of $H^+(H_2S)_n$ (n = 3 − 9) in the gas phase were characterized by means of size-selective IR spectroscopy in combination with the *ab initio* calculations. The observed structures of $H^+(H_2S)_n$ significantly differ from those of corresponding $H^+(H_2O)_n$ after the first H-bond solvation shell formation at n = 4. The charge-dipole shell formation precedes the second H-bonded shell formation. Much closely solvated structures, in which 7 molecules, at maximum, directly interact with the Eigen type ion core, are formed. The second H-bonded shell formation was confirmed to initiate at n = 9. The dissociation energy of the charge-dipole shell decreases with increasing size. The importance of dispersion in the charge-dipole shell structures was qualitatively demonstrated. The competition among intermolecular interactions was discussed to interpret the observed structures of $H^+(H_2S)_n$.

Reference

[1] L. I. Yeh, M. Okumura, J. D. Myers, J. M. Price and Y. T. Lee, *J. Chem. Phys.* 1989, **91**, 7319-7330.

[2] D. Marx, M. E. Tuckerman, J. Hutter and M. Parrinello, *Nature* 1999, **397**, 601-604.

[3] J. -C. Jiang, Y. -S. Wang, H. -C. Chang, S. H. Lin, Y. T. Lee, G. Niedner-Schatteburg and H. -C. Chang, *J. Am. Chem. Soc.* 2000, **122**, 1398-1410.

[4] J. M. Headrick, E. G. Diken, R. S. Walters, N. I. Hammer, R. A. Christie, J. Cui, E. M. Myshakin, M. A. Duncan, M. A. Johnson and K. D. Jordan, *Science* 2005, **308**, 1765-1769.

[5]G. E. Douberly, R. S. Walters, J. Cui, K. D. Jordan and M. A. Duncan, *J. Phys. Chem. A* 2010, **114**, 4570-4579.

[6] K. Mizuse and A. Fujii, *J. Phys. Chem. A* 2012, **116**, 4868-4877.

[7] N. Heine, M. R. Fagiani, M. Rossi, T. Wende, G. Berden, V. Blum and K. R. Asmis, *J. Am. Chem. Soc.* 2013, **135**, 8266-8273.

[8] I. Errea, M. Calandra, C. J. Pickard, J. R. Nelson, R. J. Needs, Y. Li, H. Liu, Y. Zhang, Y. Ma and F. Mauri, *Nature*, 2016, **532**, 81-84.

[9] H. S. Biswal, S. Bhattacharyya, A. Bhattacherjee and S. Wategaonkar, *Int. Rev. Phys. Chem.* 2015, **34**, 99-160.

[10] H. S. Biswal, P. R. Shirhatti and S. Wategaonkar, *J. Phys. Chem. A* 2010, **114**, 6944-6955.

[11] H. S. Biswal and S. Wategaonka, *J. Phys. Chem. A* 2009, **113**, 12774-12782.

[12] A. Bhattacherjee, Y. Matsuda, A. Fujii and S. Wategaonkar, *J. Phys. Chem. A* 2015, ***119,*** 1117-1126.

[13] V. R. Mundlapati, S. Ghosh, A. Bhattacherjee, P. Tiwari and H. S. Biswal, *J. Phys. Chem. Lett.* 2015, **6**, 1385-1389.

[14] *CRC Handbook of Chemistry and Physics*, 90th Edition, D. R. Lide Ed., CRC Press, Boca Raton, 2009.

[15] E. P. L. Hunter and S. G. Lias, *J. Phys. Chem*. Ref. Data 1998, **27**, 413-457.

[16] H. F. Prest, W.-B. Tzeng, J. M. Brom, Jr. and C. Y. Ng, *J. Am. Chem. Soc.* 1983, **105**, 7531-7536.

[17] T. Pradeep and C. N. R. Rao, *Chem. Phys. Lett.* 1991, **185**, 496-500.

[18] J. M. Hermida-Ramón, E. M. Cabaleiro-Lago and J. Rodríguez-Otero, *J. Chem. Phys.* 2005, **122**, 204315.

[19] S. Maeda and K. Ohno, *J. Phys. Chem. A* 2008, **112**, 2962-2968.

[20] A. Bhattacherjee, Y. Matsuda, A. Fujii and S. Wategaonkar, *ChemPhysChem* 2013, **14**, 905-914.

[21] S. Yamabe, T. Minato, M. Sakamoto and K. Hirao, *Can. J. Chem.* 1985, **63**, 2571-2574.

[22] K. Mizuse, A. Fujii, *Phys. Chem. Chem. Phys*. 2011, **13**, 7129-7135.

[23] D. H. Levy, *science* 1981, **214**, 263-269.

[24] C. B. Moore, ed., pp. 1-41, Academic Press, New York; Hayes, J. M. and Small, G. J. (1983) Anal. Chem. 55, 565A

[25] M. Miyazaki, A. Fujii, T. Ebata, N. Mikami, *Science* 2004, **304**, 1134-1137.

[26] M. J. Frisch, G. W. Trucks, H. B. Schlegel, G. E. Scuseria, M. A. Robb, J. R. Cheeseman, G. Scalmani, V. Barone, B. Mennucci, G. A. Petersson, H. Nakatsuji, M. Caricato, X. Li, H. P. Hratchian, A. F. Izmaylov, J. Bloino, G. Zheng, J. L. Sonnenberg, M. Hada, M. Ehara, K. Toyota, R. Fukuda, J. Hasegawa, M. Ishida, T. Nakajima, Y. Honda, O. Kitao, H. Nakai, T. Vreven, J. A. Montgomery, Jr., J. E. Peralta, F. Ogliaro, M. Bearpark, J. J. Heyd, E. Brothers, K. N. Kudin, V. N. Staroverov, T. Keith, R. Kobayashi, J. Normand, K. Raghavachari, A. Rendell, J. C. Burant, S. S. Iyengar, J. Tomasi, M. Cossi, N. Rega, J. M. Millam, M. Klene, J. E. Knox, J. B. Cross, V. Bakken, C. Adamo, J. Jaramillo, R. Gomperts, R. E. Stratmann, O. Yazyev, A. J. Austin, R. Cammi, C. Pomelli, J. W. Ochterski, R. L. Martin, K. Morokuma, V. G. Zakrzewski, G. A. Voth, P. Salvador, J. J. Dannenberg, S. Dapprich, A. D. Daniels, O. Farkas, J. B. Foresman, J. V. Ortiz, J. Cioslowski and D. J. Fox, GAUSSIAN 09, (Revision C.01), Gaussian Inc., Wallingford CT, 2010.

[27] L. Lechuga-Fossat, J.-M. Flaud, C. Camy-Peyret and J. W. C. Johns, *Can. J. Phys.* 1984, **62,** 1889-1923.

[28] M. R. Fagiani, H. Knorke, T. K. Esser, N. Heine, C. T. Wolke, S. Gewinner, W. Schöllkopf, M.-P. Gaigeot, R. Spezia, M. A. Johnson and K. R. Asmis, *Phys. Chem. Chem. Phys*. 2016, **18**, 26743-26754.

[29] J.-H. Choi, K. T. Kuwata, B.-M. Haas, Y. Cao, M. S. Johnson and M. Okumura, *J. Chem. Phys.* 1994, **100,** 7153-7165.

[30] T. Pankewitz, A. Lagutschenkov, G. Niedner-Schatteburg, S. S. Xantheas and Y.-T. Lee, *J. Chem. Phys.* 2007, **126,** 074307.

[31] K. Mizuse, H. Hasegawa, N. Mikami and A. Fujii, *J. Phys. Chem. A* 2010, **114**, 11060-11069.

[32] K. Fathe, J. S. Holt, S. P. Oxley and C. J. Pursell, *J. Phys. Chem. A* 2006, **110**, 10793-10798.

[33] G. A. Jeffrey, *An Introduction to Hydrogen Bonding*, Oxford University Press, New York, 1997.

[34] T. Hamashima, Y. -C. Li, M. C. H. Wu, K. Mizuse, T. Kobayashi, A. Fujii and J.-L. Kuo, *J. Phys. Chem. A* 2013, **117**, 101-107.

[35] D. Wang and A. Fujii, *Phys. Chem. Chem. Phys.* 2017, **19**, 2036-2043.

Chapter 3

Spectroscopic observation of hemibonded (two-center three-electron bonded) structures of $(H_2S)_n^+$ clusters in the gas phase

Published in *Chemical Science*, **2017**, 8, 2667-2670.

Abstract

A hemibond (two-center three-electron 2c-3e bond) is a non-classical chemical bond, and its existence has been supposed in radical cation clusters with lone pairs. Though the nature of hemibond and its role in the reactivity of the radical cation have attracted great interest, spectroscopic observations of hemibonded structures have been very scarce. In the present study, the stable hemibonded core $(H_2S\therefore SH_2)^+$ in $(H_2S)_n^+$ (n = 3 − 6) in the gas phase is demonstrated by infrared spectroscopy combined with quantum chemical calculations. The spectral feature of the free SH stretch of the ion core shows that the hemibond motif of the ion core is held up to the completion of the first H-bonded solvation shell. All the observed spectra are well reproduced by the minimum energy hemibonded isomers, and no sign of the proton-transferred type ion core H_3S^+-SH, which is estimated to have much higher energy, is found. The spin density calculations show that the excess charge is almost

equally delocalized over the two H_2S molecules in the cluster through n = 3 to 6. This also indicates the hemibond nature of the $(H_2S\therefore SH_2)^+$ ion core and small impact of the solvation shell formation on the ion core.

3.1 Introduction

As has been described in Chapter 1, even though enormous theoretical and experimental studies have been performed on hemibonded systems, our understanding of such particular chemical bonds is still limited. One of the simple model systems to investigate hemibonded radical cations is $(H_2O)_n^+$. In spite of many theoretical studies so far, however, hemibonded structures of $(H_2O)_n^+$ have not yet been experimentally observed because of the strong competition of the proton-transferred type H_3O^+-OH ion core formation.[1-4] On the other hand, $(H_2S)_n^+$ seems to be more feasible for hemibond studies.

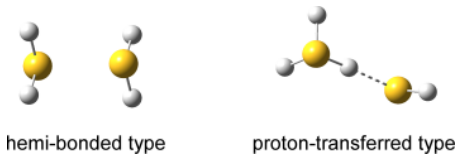

Fig. 3.1.1 Two possible structural motifs of $(H_2S)_2^+$. Reproduced from Ref. 16 with permission from the Chemical Science Owner Societies.

Theoretical calculations of the S-S hemibond have been first performed by Clark for $(H_2S)_2^+$,[5]Later on, several high level *ab inito* studies of $(H_2S)_2^+$ have been performed, and these studies have predicted that the hemibonded structure $(H_2S\therefore SH_2)^+$ is much more stable than the proton-transferred structure H_3S^+-SH (see Fig. 3.1.1) by ca. 50~100 kJ/mol,

depending on the level of theory.[6,7-9] This preference of the hemibonded type structure in $(H_2S)_2^+$ contrasts to its analogues of the period 2 elements. Furthermore, an energy decomposition scheme has been applied to $(H_2S\therefore SH_2)^+$, and its result has shown that nearly 60% of the attraction in a sulfur−sulfur bond is provided by the three-electron bond but the electrostatic interaction also makes a large contribution (~40%) to the bond.[10] This energy decomposition scheme neglects electron correlation. Therefore, we should note that dispersion may also play an important role in such a system.[11]

Apart from the theoretical studies, a few experimental studies have been reported. The first experimental observation of the sulfur-sulfur hemibond has been performed by Asmus and coworkers. They have observed the (σ, σ^*) transition of the hemibond. The electronic spectrum of $(H_2S)_2^+$ in the aqueous solution has been also reported by Asmus and coworkers, and the absorption band position well agree with the theoretical prediction. However, detailed structural information is hardly extracted from the broadened electronic transition.[12] Spectroscopic evidence in the gas phase was highly requested to examine the theoretical predictions on the sulfur-sulfur hemibond.

Recently, weakening of a hemibond through the delocalization of the spin density beyond the two nuclei centers has been suggested.[13,14] This phenomenon implies potential influence of hydrogen bonds (H-bonds) on the hemibond since charge transfer by orbital overlap frequently occurs with formation of an H-bond.[15] Influence of H-bonds (solvation) on the hemibonded ion core should be also explored.

In the present study, to address the issues proposed above, we perform infrared (IR) spectroscopy of $(H_2S)_n^+$ (n = 3 − 6) in the gas phase. The presence of the $(H_2S\therefore SH_2)^+$ hemibonded ion core is revealed for all the observed sizes, and the solvation structure evolution is characterized. The experimental observation is consistent with the superiority of the hemibonded ion core over the proton-transferred ion core in $(H_2S)_n^+$ predicted by the recent theoretical calculations.[8]

3.2 Experimental Setup

3.2.1 Overview of Infrared Photodissociation Spectroscopy

The scheme of spectroscopy and experimental apparatus are essentially the same as those described in Chapeter 2. $(H_2S)_n^+$ clusters were generated by discharge to a supersonic jet expansion of the H_2S/Ar gaseous mixture of 5 atm. Generated ions were introduced into the tandem type quadrupole mass spectrometer. The cluster size of interest was selected by the first mass spectrometer. The mass resolution was set to be higher than $\Delta m/z = 1$, and contribution of $H^+(H_2S)_n$ protonated clusters was carefully removed. Then the size-selected clusters were introduced into the octopole ion guide, therein, the clusters were irradiated by the tunable IR light from the OPO/OPA system (LaserVision) pumped by the Nd-YAG laser (Continiuum PL-8000). The fragment ions were monitored by the second quadrupole mass spectrometer. IR spectra were recorded by monitoring the fragment in the single H_2S loss channel while scanning the IR frequency in the 2300 – 2700 cm^{-1} region. The observed

spectra were normalized by the IR light power and band frequencies were calibrated by absorption lines of CO_2 and CH_4.

3.3 Results and Discussion

Fig. 3.2.1 shows the observed IR spectra of $(H_2S)_n^+$ ($n = 3 - 6$) in the SH stretch region. The bands higher than 2550 cm^{-1} are attributed to free SH stretches, and they are categorized to three different types of vibrations, as indicated by colored dotted blocks in the figure. Because of the ionization, SH bonds in the ion core should be somewhat weakened, so their stretch frequency is expected to be lower than neutral H_2S. Therefore, the lowest frequency band at around 2560 cm^{-1} in each size (the band in the red dotted block) is assigned to free SH stretches of the ion core. The frequency of this band is very close to the free SH stretch band (2558 cm^{-1}) of the H_3S^+ ion core in $H^+(H_2S)_n$ shown in the previous chapter.[16] The two relatively higher frequency bands at around 2595 and 2610 cm^{-1} (the bands in the blue and green dotted blocks) are assigned to the symmetric (ν_1) and asymmetric (ν_3) SH stretch bands of neutral H_2S moiety, respectively, which is solvating the ion core as an acceptor of an H-bond. These band frequencies are also very close to the corresponding free SH bands in $H^+(H_2S)_n$.[34] The ν_1 and ν_3 frequencies of neutral H_2S monomer have been reported to be 2614 and 2628 cm^{-1}, respectively.[17] The most striking feature in the spectra is in the free SH stretch band of the ion core highlighted by the red dotted block. Since the acidity of the SH bond in the ion core is enhanced with the charge, SH in the ion core is expected to be

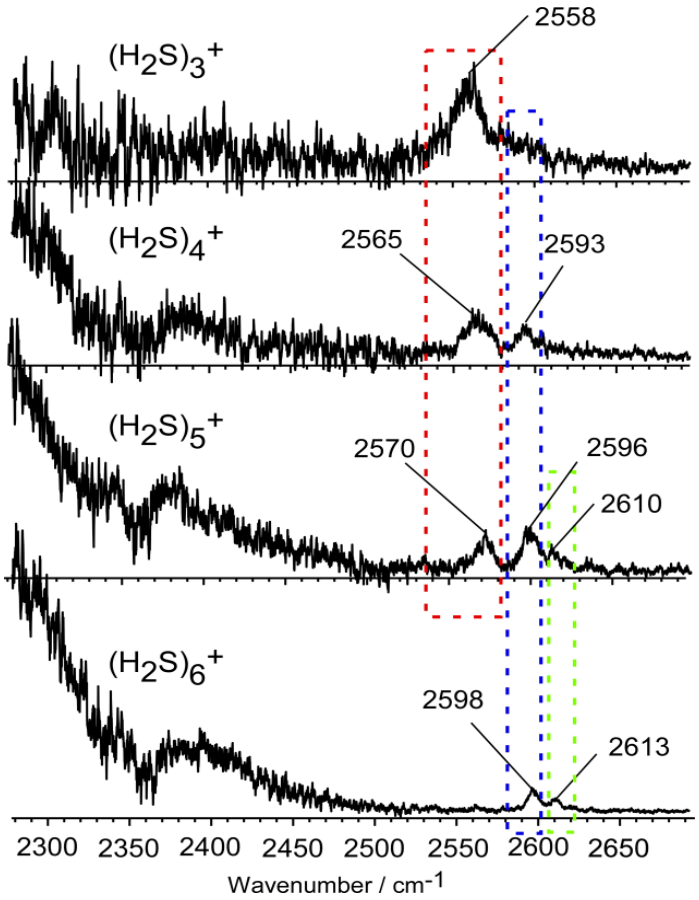

Fig. 3.2.1 Observed IR spectra of $(H_2S)_n^+$ (n = 3 − 6). The bands are categorized into three types by colored dotted blocks (see text). The bump at ~2400cm^{-1} throughout all the size is caused by the depletion at 2360 cm^{-1} due to the strong IR absorption by atmospheric CO_2. Reproduced from Ref. 16 with permission from the Chemical Science Owner Societies.

preferentially solvated (H-bonded) by neutral H_2S in the cluster. Therefore, the free SH band of the ion core should disappear when the number of neutral H_2S molecules in the cluster is enough to solvate all the SH bonds of the ion core. Whatever the ion core is the hemibonded or proton-transferred type, the free SH of the ion core should exist in $(H_2S)_3^+$. Assuming the ion core is the proton-transferred type, the free SH stretch in the core is supposed to disappear at $n = 4$.[3] In the observed spectra, however, the free SH band actually disappears at $n = 6$. This clearly demonstrates that the ion core of the clusters is the hemibonded type $(H_2S\therefore SH_2)^+$ which has four SH bonds. The solvation of the SH bonds of the hemibond ion core is completed at $n = 6$. Moreover, this result indicates that the hemibonded ion core is stable with the solvation (H-bond formation) at least up to the first solvation shell completion.

With the solvation of the hemibonded ion core, the H-bonded SH stretch band of the ion core is expected to appear in the spectra. In the region below 2300 cm^{-1}, a very broad absorption is seen, and this absorption is attributed to the H-bonded SH of the ion core. With increasing size, the weakening of the hydrogen bond of the ion core occurs as the ion core interacts with more number of H_2S molecules, and a blue-shift trend of the broad absorption appears. However, the peak position is out of the reliable measurement range of our experimental setup.

To shed light on the structures of $(H_2S)_n^+$ ($n = 3 - 6$), theoretical methods with a good balance between reliability and efficiency are requested. As confirmed in Chapter 2, the MP2/aug-cc-pVDZ level has high reliability for various neutral sulfur-centered hydrogen

bonded systems and $H^+(H_2S)_n$.[18] Unrestricted wave functions for radical cations in MP2 tend to be contaminated by states of higher spin multiplicity. However, for $(H_2S)_2^+$, it has been found that the unrestricted and restricted open-shell MP2 approaches, namely UMP2 and ROMP2, predict almost the same energy difference between the hemibonded and proton-transferred type structures, showing comparable accuracy with those of CCSD(T), and the deviation of the spin angular moment $<S^2>$ value under UMP2 and ROMP2 is in the acceptable range.[9] In the present work, besides the UMP2 method, a computational cost-effective double hybrid DFT procedure, UB2PLYPD, is also employed. By including 53% HF exchange and 27% perturbation correlation contribution, UB2PLYPD has been tested to treat spin contamination well.[19] Upon these two theoretical approaches, exhaustive conformational search generates both hemibonded and proton-transferred type low-lying structures on the potential energy surface. For all the sizes we searched, the energy separation between the two ion core motifs is larger than 40 kJ/mol and the hemibonded type is the most energetically favored one. Therefore, for the proton-transferred type isomers, only the most stable one is included in the summary of $n \geq 4$ (we should note that the structures of the proton-transferred type isomer are essentially same as those of corresponding $H^+(H_2S)_n$, which have been shown in Chapter 2). The dominance of the hemibonded type and the relative energy order are irrespective of the choice of the theoretical level, UMP2/aug-cc-pVDZ or UB2PLYPD/aug-cc-pVDZ. Details are seen in Table 3.2.1.

Table 3.2.1. Calculated relative energies in kJ/mol of the isomers of $(H_2S)_n^+$ (n = 3 − 6) at the UMP2/aug-cc-pVDZ and UB2PLYPD/aug-cc-pVDZ levels. Spin angular moment $<S^2>$ values are also shown.

Structure[a]	UMP2/aug-cc-pVDZ	$<S^2>$	UB2LYPD/aug-cc-pVDZ	$<S^2>$
3-1	0	0.7776	0	0.7609
3-2	41.6	0.7619	48.4	0.7560
3-3	44.7	0.7637	50.9	0.7569
3-4	54.6	0.7611	92.2	0.7557
3-5	80.6	0.7611	63.4	0.7556
4-1	0	0.7778	0	0.7610
4-2	4.63	0.778	0.840	0.7612
4-3	6.01	0.7759	2.76	0.7607
4-4	9.13	0.7773	N/A	N/A
4-5	42.8	0.7616	46.6	0.7559
5-1	0	0.7775	0	0.7609
5-2	3.28	0.7776	5.85	0.7610
5-3	10.7	0.7623	N/A	N/A
5-4	4.76	0.7768	8.86	0.7608
5-5	46.0	0.7611	53.4	0.7556
6-1	0	0.7780	0	0.7610
6-2	2.87	0.7774	N/A	N/A
6-3	6.01	0.7770	6.74	0.7608
6-4	46.6	0.7611	57.1	0.7556

[a] The label of the structure corresponds to those in the following Tables and Figures.

Table 3.2.2 Calculated harmonic frequencies of the isomers of $(H_2S)_4^+$ at the UMP2/aug-cc-pVDZ level. All units are in cm^{-1}. The hemibonded type isomers are scaled by 0.942 and the proton-transferred type isomer is scaled by 0.946. The corresponding experimental values are listed for comparison.

	Exp.	**4-1**	**4-2**	**4-3**	**4-4**	**4-5**[a]
stretch of H-bonded SH in the ion core		2210 2243	2166 2182	2232 2266	2150	1949 2021 2138
stretch of SH• radical						2584
stretch of free SH in the hemibonded core	2565	2565 2566	2565 2567	2555 2578	2548 2564 2585[b]	
sym. stretch of free SH in H-bonded H_2S	2593	2586 2587	2585[c] 2585[c]	2586 2588	2585[b]	2592 2593
sym. stretch of free SH in charge-dipole bound H_2S					2593	
asym. stretch of free SH in H-bonded H_2S	2610	2610 2611	2609[c] 2609[c]	2610 2612	2610	2615 2617
asym. stretch of free SH in charge-dipole bound H_2S					2618	

[a] Proton-transferred type.

[b] These two vibrational modes are heavily mixed.

[c] Degenerated frequencies.

Table 3.2.3 Calculated harmonic frequencies of the isomers for $(H_2S)_4^+$ at the UB2PLPYD/aug-cc-pVDZ level. All units are in cm^{-1}. The hemibonded type isomers are scaled by 0.9607 and the proton-transferred type isomer is scaled by 0.963. The corresponding experimental values are listed for comparison.

	Exp.	**4-1**	**4-2**	**4-3**	**4-5**[a]
stretch of H-bonded SH in the ion core		2144 2195	2094 2126	2161 2194	1884 1963 2107
stretch of SH• radical					2580
stretch of Free SH in the hemibonded core	2565	2576 2577	2574 2576	2568 2582	
sym. stretch of H-bonded H_2S	2593	2593[b] 2593[b]	2587[b] 2587[b]	2590 2591	2593 2594
asym. stretch of H-bonded H_2S		2608[b] 2608[b]	2603[b] 2603[b]	2606[b] 2606[b]	2608 2609

[a] Proton-transferred type

[b] Degenerated frequencies

The essentially same conclusion has also been reported by Do *et al*. for $(H_2S)_n^+$ (n=2-4) by searching the isomers through the Basin-Hopping approach and structural optimization at CCSD(T)/aug-cc-pVDZ.[8] In our computations, the UMP2 method yields the $<S^2>$ value with small deviation of 0.021 at average to the exact value (0.75) and the spin contamination is not serious. Furthermore, the simulated spectra by the UMP2 method show better agreement with the experimental ones than those by UB2PLYPD. Details are shown in Tables 3.2.2 and 3.2.3. Thus, in the following, UMP2/aug-cc-pVDZ is utilized as the main theoretical method.

In Fig. 3.2.2 to 3.2.5, we compare the observed IR spectra of $(H_2S)_n^+$ (n = 3 − 6) with the harmonic simulated spectra of the stable isomers. In addition, the simulated spectrum of the most stable isomer of each size, which is actually in the best agreement with the experimental spectrum, is summarized in Fig. 3.2.6. The most stable isomer in each size has the hemiboned type ion core. The stick harmonic spectra are convoluted with a Lorentzian function of 10cm^{-1} FWHM, and the frequencies are scaled by the factor 0.942. The simulations reproduce well the observed spectra, supporting the qualitative assignments provided above. For the ν_3 band, non-negligible discrepancy between the observed spectra and simulations is found. The observed ν_3 band intensity, relative to ν_1, seems to be remarkably suppressed. The similar suppression of the ν_3 band has been also seen in $H^+(H_2S)_n$ and many water analogues. This has been ascribed to difference of the internal rotation structure, dissociation yield, and transition intensity enhancement between the ν_1 and ν_3 bands, as discussed in Chapter 2.[16,20-22]

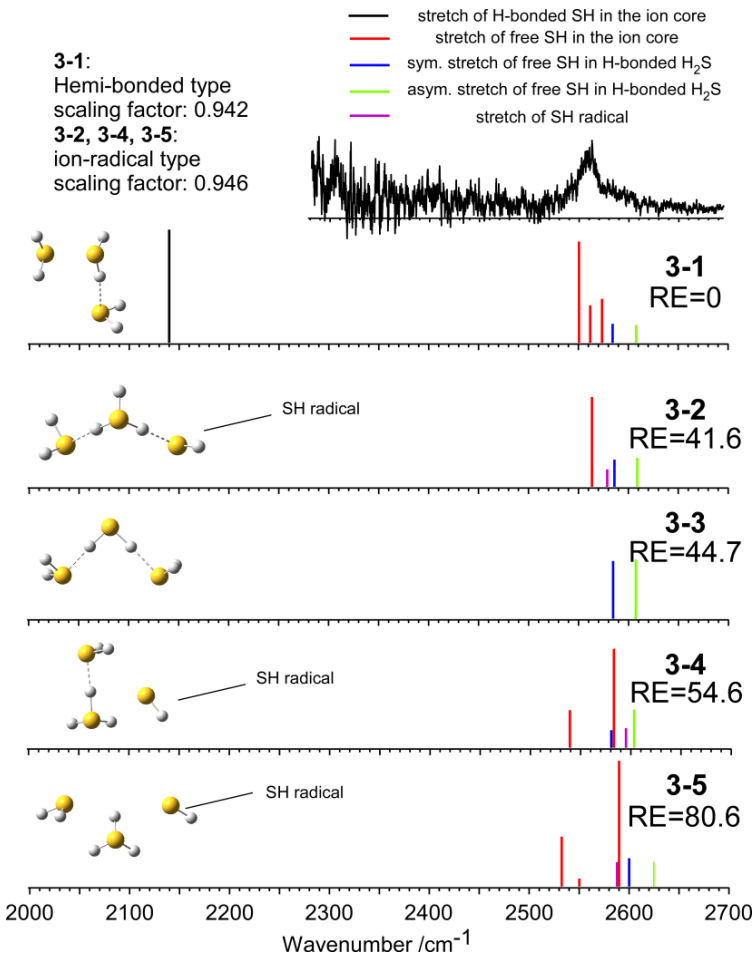

Fig. 3.2.2. Comparison between the observed and simulated spectra of $(H_2S)_3^+$. Colors of the sticks represent types of stretch modes, and they are shown on the top of the panel. Relative energy (RE) is also shown in kJ/mol. Since the intensity of the stretch of H-bonded SH in the ion core is about 100~400 times greater than those of the free SH stretches in the neutral H_2S moiety, its stick is simply cut for a clear presentation. The stretch frequencies of H-bonded SH in the ion core of **3-2**, **3-3** and **3-4** are out of the displayed range; 1690 and 1945 cm^{-1} for **3-2,** 1573 and 1754 cm^{-1} for **3-3**, and 1368 cm^{-1} for **3-4.** Reproduced from Ref. 16 with permission from the Chemical Science Owner Societies.

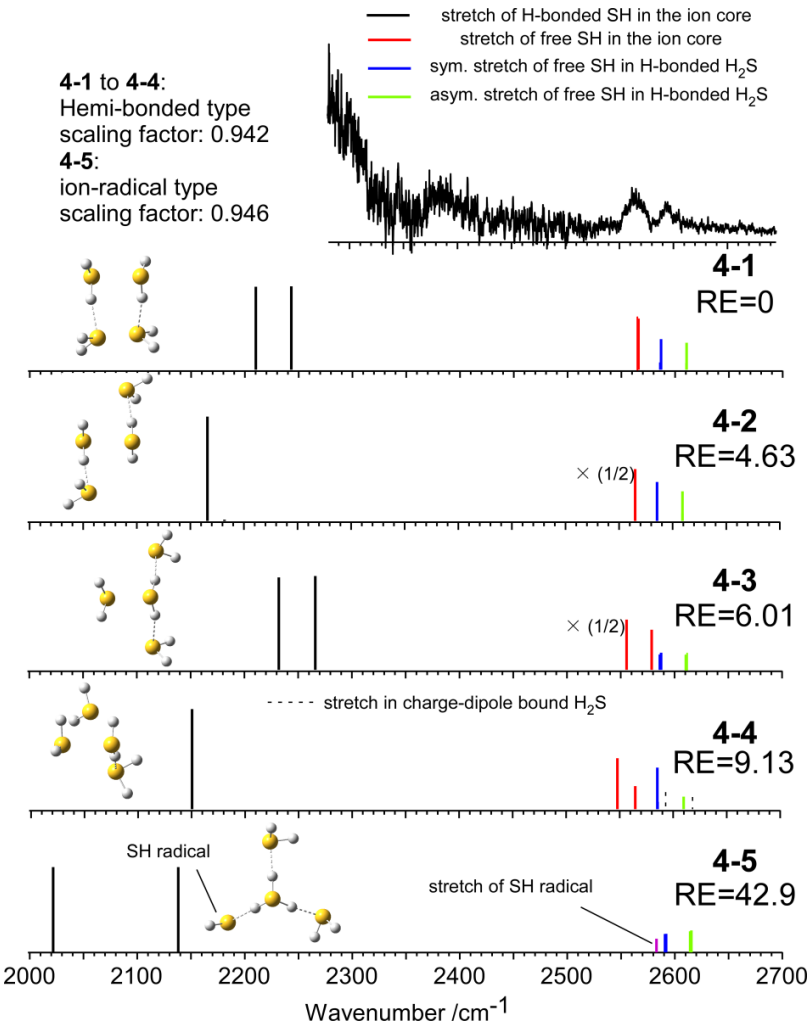

Fig. 3.2.3. Comparison between the observed and the simulated spectra for $(H_2S)_4^+$. Colors of the sticks represent types of stretch modes, and they are shown on the top of the panel. Relative energy (RE) is also shown in kJ/mol. Since the intensities of the stretches of H-bonded SH in the ion core are about 100~400 times greater than that of the free SH stretches in the neutral H_2S moiety, their sticks are simply cut for a clear presentation. The two bands of stretches of H-bonded SH in the hemibonded core of **4-2** are degenerated. Another stretch of H-bonded SH in the ion core of **4-5** is located at 1949 cm^{-1}. For **4-4**, one H_2S is bound to the hemibonded ion core by the charge-dipole interaction. Reproduced from Ref. 16 with permission from the Chemical Science Owner Societies.

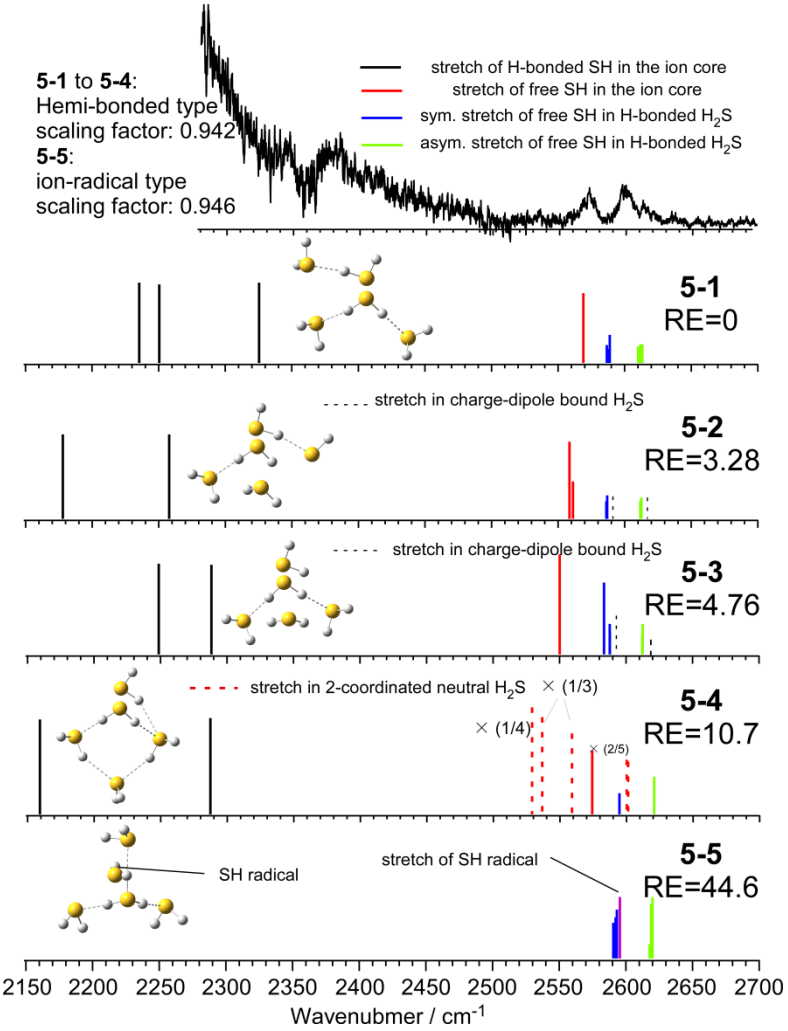

Fig. 3.2.4 Comparison between the observed and the simulated spectra for $(H_2S)_5^+$. Colors of the sticks represent types of stretch modes, and they are shown on the top of the panel. Relative energy (RE) is also shown in kJ/mol. Since the intensities of the stretches of H-bonded SH in the ion core are about 100~400 times greater than that of the free SH stretches in the neutral H_2S moiety, their sticks are simply cut for a clear presentation. In **5-2** and **5-3**, there are the stretch vibrational modes of charge-dipole bound H_2S, which are denoted by black dotted lines. In **5-4**, the SH stretches arising from the 2-coordinated H_2S sites are denoted by red dotted lines. The stretches of H-bonded SH in the ion core of **5-5** locate at 1889, 2011, and 2106 cm^{-1}. Reproduced from Ref. 16 with permission from the Chemical Science Owner Societies.

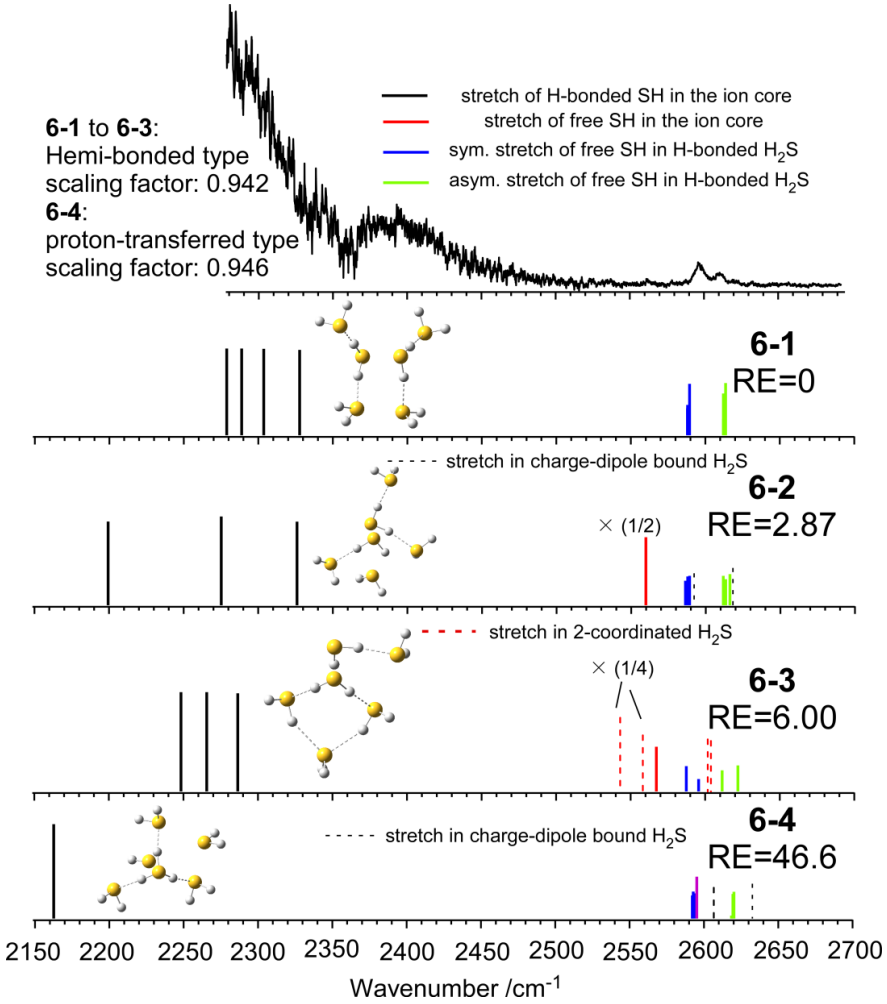

Fig. 3.2.5 Comparison between the observed and the simulated spectra for $(H_2S)_6^+$. Colors of the sticks represent types of stretch modes, and they are shown on the top of the panel. Relative energy (RE) is also shown in kJ/mol. Since the intensities of the stretches of H-bonded SH in the ion core are about 100~400 times greater than that of the free SH stretches in the neutral H_2S moiety, their sticks are simply cut for a clear presentation. For **6-2** and **6-4**, there are the stretch vibrational modes of charge-dipole bound H_2S, which are denoted by black dotted lines. The stretches arising from the 2-coordinated H_2S sites in **6-3** are denoted by red dotted lines. Another two stretches of H-bonded SH in the ion core of **6-4** locate at 1897 and 1995 cm^{-1}. Reproduced from Ref. 16 with permission from the Chemical Science Owner Societies.

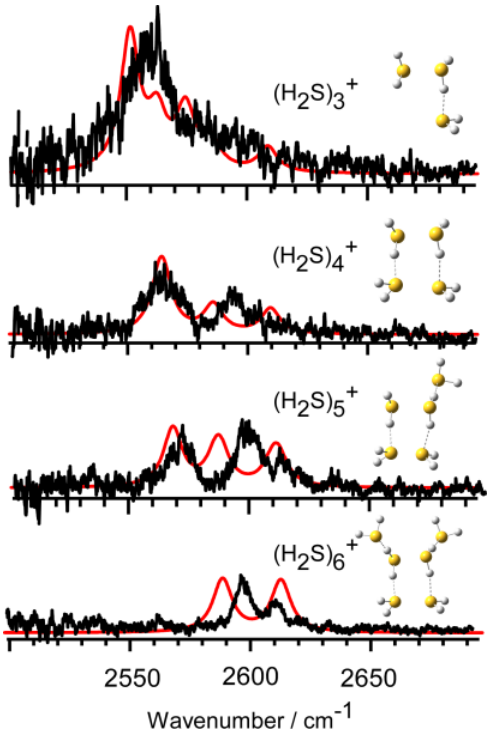

Fig. 3.2.6 Comparison between the observed spectral and harmonic spectra of the most stable isomers of $(H_2S)_n^+$ (n = 3 − 6) in the free SH region. The simulation was performed at UMP2/aug-cc-pVDZ with the scaling factor 0.942. Reproduced from Ref. 16 with permission from the Chemical Science Owner Societies.

The spin density of the most stable structures is shown in Fig. 3.2.7. The spin density (unpaired electron) is almost equally delocalized on the two H_2S molecules, indicating the 2c-3e bond nature of the ion core. With the solvation of the ion core, the positive charge gradually delocalizes to the solvent H_2S moiety. Even under the first solvation shell completion at n = 6, however, the natural charge in the $(H_2S\therefore SH_2)^+$ ion core is predominant, and this demonstrates the stability of the hemibond to the solvation (H-bond formation). The influence of the charge is also seen in the dissociation energy (D_0)

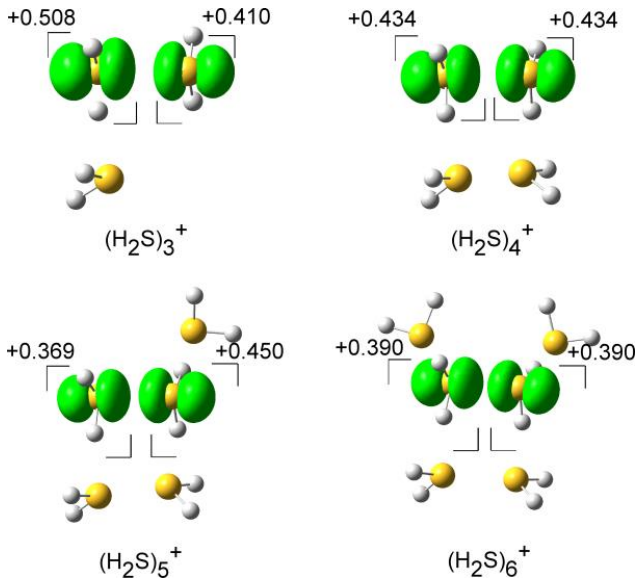

Fig. 3.2.7 The spin density for $(H_2S)_n^+$ (n = 3 − 6) (isovalue = 0.006), and the natural population analysis (NPA) charge distribution for the molecular component. Reproduced from Ref. 16 with permission from the Chemical Science Owner Societies.

calculated with the basis set superposition error (BSSE) and zero point energy corrections. D_0 is estimated to be 32.1, 30.2, 24.6, and 22.6 kJ mol^{-1} for n = 3 to 6, respectively. The gradual decrease reflects the charge delocalization of the ion core to the solvent H_2S molecules. The D_0 values of $(H_2S)_n^+$ are lower than those of $H^+(H_2S)_n$, wherein D_0 in the first H-bonded solvation shell is 42.3 kJ/mol at the same level of theory.[23] This is rationalized by the fact that the charge in $H^+(H_2S)_n$ is primarily distributed to the single molecule of the Eigen type core H_3S^+ while the charge in $(H_2S)_n^+$ is shared by the two H_2S molecules of the hemibonded ion core.

3.4 conclusions

In summary, through an IR spectroscopic study of the SH stretch region, we have experimentally proven the hemibonded motif of the ion core in $(H_2S)_n^+$ (n = 3 – 6) which has been predicted by the theoretical calculations and electronic spectroscopy. In $(H_2S)_n^+$, the hemibonded ion core motif is much more stable than the proton transferred ion core motif. The hemibonded ion core motif is stable toward solvation at least up to the completion of the first solvation shell.

Reference

[1] G. H. Gardenier and M. A. Johnson, *J. Phys. Chem. A* 2009, **113**, 4772-4779.

[2] P.-R. Pan, Y.-S. Lin, M.-K. Tsai, J.-L. Kuo and J.-D. Chai, *Phys. Chem. Chem. Phys.*2012, **14**, 10705-10712.

[3] J. D. Herr, J. Talbot, and R. P. Steele, *J. Phys. Chem. A* 2015, **119**, 752-766.

[4] K. Mizuse and A. Fujii, *J. Phys. Chem. A* 2013, **117**, 929-938.

[5] T. Clark, *J. Comput. Chem.* 1981, **2**, 261-265.

[6] P. M. W. Gill and L. Radom, *J. Am. Chem. Soc.* 1988, **110**, 4931-4941.

[7] T. K. Ghanty and S. K. Ghosh, *J. Phys. Chem. A* 2002, **106**, 11815-11821.

[8] H. Do and N. A. Besley, *Phys. Chem. Chem. Phys*. 2013, **15**, 16214-16219.

[9] T. Stein, C. A. Jiménez-Hoyos and G. E. Scuseria, *J. Phys. Chem. A* 2014, **118**, 7261-7266.

[10] F. M. Bickelhaupt, A. Diefenbach, S. P. de Visser, L. J. de Koning and N. M. M. Nibbering, *J. Phys. Chem. A* 1998, **102**, 9549-9553.

[11] P. R. Horn, Y. Mao, and M. Head-Gordon, *J. Chem. Phys*. 2016, **144**, 114107.

[12] S. A. Chaudri, K.-D. Asmus, *Angew. Chem. Int. Ed.*1981, **20**, 672-673.

[13] S. Zhang, X. Wang, Y. Sui and X. Wang, *J. Am. Chem. Soc.* 2014, **136**, 14666-14669.

[14] C. H. Hendon, D. R. Carbery and A. Walsh, *Chem. Sci.* 2014, **5**, 1390-1395.

[15] E. Ronca, L.Belpassi and F. Tarantelli, *ChemPhysChem* 2014, **15**, 2682-2687.

[16] D. Wang and A. Fujii, *Phys. Chem. Chem. Phys.* 2017, **19**, 2036-2043.

[17] L. Lechuga-Fossat, J. M. Flaud, C. Camy-Peyret and J. W. C. Johns, *Can. J. Phys.* 1984, **62**, 1889-1923.

[18] H. S. Biswal, S. Bhattacharyya, A. Bhattacherjee and S. Wategaonkar, *Int. Rev. Phys. Chem.* 2015, **34**, 99-160.

[19] A. S. Menon and L. Radom, *J. Phys. Chem. A* 2008, **112**, 13225-13230.

[20] Y. S. Wang, H. C. Chang, J. C. Jiang, S. H. Lin, Y. T. Lee, and H. C. Chang, *J. Am. Chem. Soc.* 1998, **120**, 8777-8788.

[21] T. Pankewitz, A. Lagutschenkov, G. Niedner-Schatteburg, S. S. Xantheas and Y.-T. Lee, *J. Chem. Phys.* 2007, **126**, 074307.

[22] K. Mizuse, H. Hasegawa, N. Mikami and A. Fujii, *J. Phys. Chem. A* 2010, **114**, 11060-11069.

[23] M. Bonifačić, K.-D. Asmus, J. Chem. Soc. Perkin Trans. II 1980, 758-762.

Summary

In this thesis, in order to illustrate the nature of sulfur-centered intermolecular interactions, the structures of $H^+(H_2S)_n$ (n = 3 – 9) and $(H_2S)_n^+$ (n = 3 – 6) in the gas phase were characterized by infrared spectroscopic observation and *ab initio* calculations. The structural information of the proposed models provides a significant and in-depth understanding of stabilization of protein structures and radical chemistry, since sulfur-centered intermolecular interactions are ubiquitous in protein. For example, sulfur exists in the amino acids, cysteine and methionine, and it could form the S ∴ π and S ∴ S hemibonds with the neighboring aromatic ring and amino acid, such hemibond plays a critical role in electron hopping in proteins.

We found that, in $H^+(H_2S)_n$ (n = 3 – 9), the charge-dipole shell formation precedes the second H-bonded shell formation, that means 7 molecules could directly interact with the Eigen type ion core, and the second H-bonded shell starts at size n=9. The role of dispersion and the charge-induced dipole were conceived to be critical in such closely solvated structures. In $(H_2S)_n^+$ (n = 3 – 6), the hemibonded motif of the ion core was demonstrated, as well as the small impact of the formation of a solvation shell on the ion core structure.

As for the future work, we are aimed at the spectroscopic characterization of S−H••• π interaction in the simplest model system, benzene-H_2S, in the gas phase. The noncovalent interactions involving the aromatic ring in amino acids are important in the dynamics of protein folding, while, S−H•••π interaction has rarely been investigated with only large

theoretical calculations and one investigation of rotational spectra. The dearth experimental observation is in need.